I THE PERMEABILITY OF A BED OF SMOOTH SPHERICAL PARTICLES

II NON-STEADY FLOW OF GAS THROUGH A POROUS WALL

Thesis by

Leon Green, Jr.

In Partial Fulfillment of the Requirements

For the Degree of

Doctor of Philosophy

California Institute of Technology

Pasadena, California

1949

ACKNOWLEDGMENTS

The author wishes to express his deep appreciation for the advice and constant encouragement given him by Professor Pol Duwez during the course of the present investigation. The author is also indebted to Professor Duwez and Professor Louis Dunn for extending to him the facilities of the Jet Propulsion Laboratory for the prosecution of the experimental program. In addition, the assistance of Miss Margaret Sturges, Mr. Orley Seekatz, and Mr. Howard Hill is gratefully acknowledged.

The second part of this work was made possible by the contributions of Professor Charles Wilts, to whom the author's thanks are extended.

ABSTRACT

Part I

The resistance of a bed of smooth spherical particles to gas flow in both the Darcy and quasi-turbulent regimes was investigated experimentally in order to check the accuracy of two conflicting resistance equations widely reported in the literature. Variations in specific surface and porosity of the bed independent of one another were realized by the use of spheres of different sizes systematically packed in different configurations. The experimental results are correlated on the basis of a general pressure drop equation defining two length parameters which are necessary for complete characterization of an arbitrary porous structure. These results are used to extend the range of validity of the more accurate of the two conflicting sphere bed resistance expressions. A general definition of the Reynolds number of a fluid flowing through a porous structure of arbitrary complexity is suggested, and the special conditions which permit a sphere bed to be characterized by a single length parameter are discussed.

Part II

The results of a calculation of the time required for establishment of steady flow of gas through a porous wall following the sudden application of a pressure difference across the wall are presented in dimensionless form. The calculation was made by using an electrical analogy to satisfy the non-linear partial differential equation governing the pressure distribution in the wall.

TABLE OF CONTENTS

PART I THE PERMEABILITY OF A BED OF SMOOTH SPHERICAL PARTICLES

LIST OF TABLES

PART I

PART II

LIST OF FIGURES

PART I

PART I

THE PERMEABILITY OF A BED OF SMOOTH SPHERICAL PARTICLES

I INTRODUCTION

A method of coping with the high rates of heat transfer encountered in the field of jet propulsion consists of making the parts to be cooled of a porous material and forcing the cooling fluid through the pores in a direction opposite to that of the heat flow. This method has become known as "sweat cooling" (1). Perhaps the most suitable method for fabricating porous sections for sweat cooling applications involves the use of powder metallurgy techniques (2). The principle of the method of preparing porous metals for such use consists of adding to the metal powder a powdered substance that decomposes into a gaseous phase at a temperature below the sintering temperature of the metal. The two powders are intimately mixed, pressed in a die in order to form a compact, then sintered at high temperature. When the non-metallic powder decomposes, empty spaces are left in the interior of the compact. Since the gases generated by the decomposition of the porosity-forming material must escape, small channels are formed in the compact and the pores are therefore interconnected. Although some of these channels may be closed during the sintering of the metal powder, enough of them remain open to render the metal permeable.

In designing a sweat cooled part, it is imperative to assure a certain rate of flow of coolant under given conditions of pressure drop. Such design requires knowledge of the permeability of the metal of which the part is to be made. The complexity of the metal structure, of course, precludes any analytical approach to the

problem of predicting the permeability. In the course of an experimental study of the flow of gas through different porous metal specimens conducted at the Jet Propulsion Laboratory (2), it was found that for a given metal prepared under a fixed set of conditions of compaction and sintering, the permeability coefficient (defined on the basis of Darcy's law) is a unique function of the metal porosity. A more general correlation of the measured permeability values obtained from different metals could not be realized, however.

The permeability problem in the case of porous metals of the type described above is complicated by the fact that the method of manufacture produces some porosity which does not effect permeability. That is, not all of the pores or channels are necessarily continuous throughout the metal specimen; some may be "dead ends". As the porosity of the metal is increased, the proportion of continuous or connected pores also increases, and so the permeability is doubly sensitive to porosity changes, often varying as rapidly as the tenth power of the porosity.

Another complication is introduced by the fact that Darcy's law, which defines the permeability coefficient, is valid only for viscous laminar flow. The limiting rate of flow at which the flow ceases to be truly viscous in nature can be expressed in the case of a porous medium, as well as for pipes, by a critical Reynolds number. In the case of porous metals prepared by the technique described above, however, it is not possible by inspection to define the characteristic length entering into the Reynolds number expression.

The two complicating factors mentioned above made it desirable

to approach the porous metal permeability problem by first studying the behavior of a medium possessing both continuous porosity and a well defined characteristic length, a medium which might serve as a basis for comparison. The simplest such system, and one which had been subjected to considerable scrutiny by a large number of investigators, was a bed of smooth spherical particles. Examination of the literature, however, revealed incomplete understanding of even this system. It was found that the general topic of granular beds was the subject of considerable controversy, primarily concerning the effect of bed porosity upon the resistance to flow. Two major schools of thought on this subject are extant, each with its own porosity function supported by large amounts of experimental data. In view of this situation, it was felt that further experimental work upon sphere beds was desirable.

II REVIEW OF PREVIOUS WORK

A. The Pipe Flow Analogy

The physical principles governing the flow of fluids through porous media were first investigated by Darcy (3) in 1856. His experiments on the flow of water through sands established that the rate of flow of a liquid through a unit area of porous material is directly proportional to the pressure drop per unit length of the material. This statement, known as Darcy's law, was subsequently shown to hold for the flow of gases as well as liquids, and was found to be strictly valid only in the regime of flow in which pressure losses occur as a result of viscous tangential shearing stresses arising in laminar "creeping" motion of the fluid. The similarity of Darcy's law to Poiseuille's law for the laminar flow of a viscous fluid through a capillary tube led many subsequent investigators to base their work upon the assumption that a granular bed is analogous to a group of capillaries parallel to the direction of flow. For such a hypothetical bed the porosity (defined as the ratio of void volume to total volume) of a layer normal to the direction of flow will be equal to the porosity, ε , of the bed as a whole. Since, for each such layer, the fractional free volume will be equal to the fractional free area, continuity considerations require that the apparent bulk velocity, u , of the fluid be less than the actual velocity in the pores, u_e , which would be u/ε . This assumption was originally made by Dupuit (4) in 1863 and equations based upon it are still in use. A number of attempts were made to

derive Darcy's law by application of the fundamental hydrodynamical equations to beds of hypothetical configuration, but none was successful. More useful results were obtained by the semi-empirical method of plotting by dimensionless groups.

In such an approach it was desirable to follow the example of the case of pipe flow, for which a unique correlation is obtained by plotting a dimensionless resistance coefficient against a Reynolds number:

$$\left(\frac{\tau}{\rho u_e^2}\right) = f\left(\frac{\rho u_e \frac{A}{P}}{\mu}\right)$$

where τ = shearing stress at wall

u_e = effective interstitial fluid velocity

A/P = effective "hydraulic radius"

ρ = fluid density

μ = fluid viscosity.

In order to evaluate the interstitial velocity and the hydraulic radius, however, further assumptions were necessary, and here again the Poiseuille flow analogy of Dupuit was invoked in assuming that

and that

$$\frac{A}{P} = \frac{\text{cross section area}}{\text{wetted perimeter}} \times \frac{\text{length}}{\text{length}} = \frac{\text{free volume}}{\text{wetted area}} \div \frac{\text{total volume}}{\text{total volume}} = \frac{\epsilon}{S}$$

where S = surface area of bed per unit volume of bed. In terms of the "specific surface" of the bed, S_0, defined as surface area per unit particle volume,

$$\frac{A}{P} = \frac{\varepsilon}{S_o (1-\varepsilon)} = \frac{\text{unit volume of pore space}}{\text{surface area}}$$

This representation was originally proposed by Kozeny (5) in 1927 and later worked out independently by Fair and Hatch. (4) Writing the surface shearing stress as

$$\tau = \frac{\Delta p}{L} \frac{\varepsilon}{S} = \frac{\Delta p}{L} \frac{\varepsilon}{S_o (1-\varepsilon)}$$

the fact that in the viscous regime

$$\left(\frac{\tau}{\rho u_e^2} \right) \left(\frac{\rho u_e A}{\mu P} \right) = \text{const.}$$

was used to derive an equation for the pressure gradient across a layer of a porous medium as a function of the porosity and specific surface of the bed and the bulk velocity of flow through it which is generally known as Kozeny's equation:

$$\frac{\Delta p}{L} = k \mu S_o^2 \frac{(1-\varepsilon)^2}{\varepsilon^3} u \qquad (1)$$

where k is a dimensionless constant equal to about 5.0.

This equation has been applied by Carman (7,8) to the measurement of the specific surface of beds of porous material and is also used in filtration theory. A similar equation later given by Fair and Hatch (6, 9, 10, 11) is

$$\frac{\Delta p}{L} = k \rho \left(\frac{u}{\varepsilon} \right)^n (S_o)^{3-n} \left(\frac{\varepsilon}{1-\varepsilon} \right)^{n-3} \left(\frac{\mu}{\rho} \right)^{2-n} \qquad (2)$$

where the exponent n is a "state of flow factor" which varies

from 1 in viscous laminar flow to 2 in the case of "turbulent" flow. For n = 1, the Fair-Hatch and Kozney equations are identical.

B. The Dimensional Approach

It would appear evident that the idealized Dupuit model upon which the above equations are based cannot accurately represent the true complexity of a granular bed. The validity of the Kozeny theory has been challenged by Bakhmeteff and Feodoroff (12, 13, 14, 15) who, arguing from dimensional considerations, point out that for a generalized porous medium (as opposed to the Dupuit model) the fractional free cross sectional area is not necessarily equal to the fractional void volume, and propose that the interstitial void velocity should be not u/ε, but rather $u/\varepsilon^{2/3}$. Such considerations lead to a pressure gradient equation corresponding to that of Fair-Hatch of the form

$$\frac{\Delta p}{L} = k' \rho u^n S_o^{3-n} \left(\frac{\mu}{\rho}\right)^{2-n} (\varepsilon)^{-\frac{n+3}{3}} \qquad (3)$$

Bakhmeteff and Feodoroff do not attempt to criticize the structure of the Fair-Hatch equation (the idealized basis for which should prove inadequate for flows beyond the viscous regime), but merely point out that the two equations disagree as to the effect of porosity. Their discussion is limited to the case of viscous laminar flow (n = 1), for which case the "porosity functions" of the two equations reduced to numerical terms (15), become

Fair-Hatch: $$f(\varepsilon) = 358\ \frac{(1-\varepsilon)^2}{\varepsilon^3}$$

(4)

Bakhmeteff-Feodoroff: $$f(\varepsilon) = \frac{640}{\varepsilon^{4/3}}$$

A graph of these two functions, taken from Ref. 11, is presented in Figure 1. It would be expected that the existing experimental data on granular beds would verify one of the above functions and disprove the other. This is not the case, however, since a considerable number of data can be marshalled in support of each theory. In view of such contradicting evidence, Bakhmeteff and Feodoroff conclude that the problem can be resolved only by further experimental work.

It is the opinion of the writer that the above difficulty is at least partly attributable to two main factors. The first of these is the small range of porosity encompassed by the usual experiments with beds of smooth round particles. In a random packing of spheres, such as was used in the work mentioned above, only a limited variation in bed porosity is easily attainable. Carman (16) reports that in large containers with good vibration, spherical particles tend to pack together with a porosity of about 39 per cent, which is practically constant for all particle sizes. Figure 1, however, shows that this is almost exactly the point at which the two porosity functions agree, and so it may be understood how studies with bed porosities varying only slightly from 39 per cent might not provide sufficient basis for a choice between the two conflicting expressions.

Supporters of the Kozeny or Fair-Hatch theory will point out in the connection that it has been experimentally verified over a wide range of porosities. Examination of the data, however, reveals that in the supporting experiments the porosity range was extended by changing the nature of the bed material. It would appear that such studies, which utilized media like wire spirals and Berl saddles to obtain high bed porosities, and realized low porosities by the use of such materials as closely bedding mica flakes, cannot provide a firm support for the Kozeny expression, since sufficient control of the specific surface of the bed was not maintained. Any comparison of the two porosity functions of Equations (6) requires that the specific surface be held constant, and the lack of such control in many of the experimental investigations constitutes the second factor tending to confuse the problem.

C. Representation of the State of Flow

The two pressure gradient expressions presented above take consideration of the flow regime by including the exponent n as a "state of flow factor" which may assume values greater than 1 in the transition zone above the Darcy region and may reach a value of 2. The pipe analogy school of thought explains the smooth transition by assuming that the parallel tubes of the Dupuit model may vary in size, so that turbulent flow may be realized in the larger tubes while laminar conditions still prevail in the smaller ones. This explanation appears unsatisfactory, however, since the granular bed experiments show that the transition from the Darcy regime begins

at a rate of flow characterized by a Reynolds number (based on particle diameter) of the order of 1. The existence of conditions of true turbulent mixing within the interstices of the bed at such a low Reynolds number is highly improbable, and references to the state of flow characterized by $n > 1$ as necessarily "turbulent" (an adjective too frequently encountered in the literature on the subject) may be misleading.*

Bakhmeteff and Feodoroff, on the other hand, make a precise distinction in this connection by pointing out that a more correct analogy would be not to Poiseuille flow in pipes, for which inertia terms simply do not appear in the equations, but rather to the movement of a fluid around a sphere, in which case the equations are solved in the Stokes approximation only by the quantitative assumption, valid within certain limits, that the inertia terms containing the quadratic velocity elements may be neglected. According to this analogy, the Darcy regime corresponds to the realm of validity of the Stokes approximation in which the inertia forces are negligible compared to the viscous forces. At higher rates of flow, however, no matter whether the flow is turbulent or laminar, the contribution of the forces arising from the inertia of the fluid becomes more predominant until finally the quasi-turbulent regime is reached.

The above analysis of the mechanism of resistance of a granular bed to fluid flow was apparently first made by Forcheimer. Considering

---

* A further discussion of this matter is given in Section III B.

the fact that the viscous forces are proportional to the first power of the velocity and the inertial forces are proportional to the second power, Forcheimer (17) suggested that the pressure gradient through the bed might best be represented by a simple quadratic equation of the form

$$\frac{\Delta p}{L} = au + bu^2 \tag{5}$$

This method of representation seems particularly appropriate in view of the long range of gradual flow transition in which both the linear and quadratic terms are of comparable importance, as contrasted to the relatively abrupt transition from laminar to turbulent flow in pipes. Nevertheless, most recent investigators (perhaps with the exception of Chalmers, Taliaferro, and Rawlins) (18) apparently have seen fit to ignore Forcheimer's quadratic equation and to correlate their data in terms of the friction factor versus Reynolds number representation conventional in pipe flow problems. Although such a method may be satisfactory for use with beds of smooth sphere-like particles, packings of more complicated shapes again introduce the problem of evaluating the Reynolds number, and thus involve considerable difficulty. In an effort to avoid this problem, the present investigation will seek a correlation based upon an equation of the Forcheimer type, not only because the two-term equation provides a more realistic picture of the resistance mechanism, but also because it introduces the possibility of defining a Reynolds number for porous media whose structures defy

description, as will be discussed in Section VI.

D. The Wall Effect

The work of a number of investigators as reported in the literature substantiates the belief that the resistance of a granular bed to the flow of a fluid is influenced by the size of the tube into which the bed is packed. There appears to be no unanimous agreement, however, as to whether the effect of the walls is to increase or decrease the resistance to flow, although it is agreed that variations of resistance due to wall effect become small as the ratio of the flow tube diameter to the packing particle diameter increases. In an experimental investigation such as the present one, therefore, the wall effect might ideally be made completely negligible by the use of flow channels of dimensions large compared to the sphere diameter. Practical considerations, however, such as the capacity of the available flow measuring equipment, the cost of spherical particles of an easily handled size, and the difficulty involved in packing the bed, indicated that the flow tube dimensions would have to be limited to a size which would involve a noticeable wall effect. Other means, therefore, were required in order either to minimize the magnitude of the wall influence or to render it calculable.

A study of the literature showed that all the experiments with granular beds for which data were reported had been performed with flow tubes of circular cross section.* Photographs of the cross

* The only apparent exception to this statement is the unpublished work mentioned briefly by Ruth (19).

sections of beds packed inside such tubes (20, 21) reveal that the porosity of the bed is greater in the layers next to the wall than in those nearer the middle of the bed. Such non-uniformity of the bed, due to "bridging" of the particles, becomes more pronounced as the ratio of tube diameter to particle diameter decreases. Two oppositely directed influences exerted by the presence of the container wall may therefore be distinguished.

First, the increased porosity of the layers next to the wall indicates that the permeability of the bed should be higher at the periphery than near the center. The presence of the wall, on the other hand, provides additional surface which should result in increased fluid friction. The fact that these two effects tend to counteract one another may be in part responsible for the variety of the "wall corrections" reported in the literature. The effect of the increased bed porosity near the container wall has been investigated mathematically (20, 22), but the arguments are tenuous at best. The effect of the additional wall friction has been taken into account by assuming that the resistance to flow would be proportional to the sum of the area of the bed material and the area of the container wall. A widely reported method of wall correction (which apparently allows for the partial compensation of the two oppositely directed effects) is that suggested by Carman (8), which is a strictly arbitrary correction based on the fact that he obtained a better fit of his own and other experimental data by adding but half the area of the container to the area of the bed material.

This approximate empirical correction was not thought sufficiently accurate for the present investigation, however, since the nature of the wall effect may be variable, depending upon the flow regime obtaining within the bed (20, 22). In the Darcy regime the energy losses are due to the viscous stresses in the fluid and so should be proportional to the velocity gradient and to the area of the surface upon which the stresses act. For this case of viscous flow, it would appear that the actual particle distribution should be of secondary importance, that the resistance of the bed should be proportional to the total exposed area, and that the correct compensation for wall effect should be to add the entire wall area. In the case of flows at high Reynolds numbers, however, such an explanation is not sufficient, since it is evident that the distribution of the particles in the bed influences the tortuosity of the bed, which will have great effect upon the inertia forces which predominate at high rates of flow.

From the above considerations it was felt that in the present investigation a sufficiently accurate correction for the additional friction afforded by the container wall could easily be made. It was judged, however, that the complexity of the effect of the non-uniform particle distribution near the wall upon the inertial resistance would preclude any method of rational compensation, and that a more practical line of approach would be an attempt to render this type of wall effect negligible by packing the bed in a mode compatible with the boundary shape and by filling the voids at the tube wall

with properly shaped inserts. Only one such attempt is apparent in the literature (19) but it was mentioned only briefly and no experimental data were given.

III THE PRESSURE DROP EQUATION

A. Derivation of the Equation

In the case of a viscous liquid flowing linearly through a porous medium, dimensional considerations proposed by Muskat (23) show that when changes in elevation are neglected, the pressure gradient in the system may be expressed as

$$-\frac{dp}{dL} = \text{const.}\ \frac{\mu^2}{\rho \delta^3}\ F\left(\frac{\delta \rho u}{\mu}\right) \tag{6}$$

where u = average velocity ?

ρ = density of fluid

μ = viscosity of fluid

δ = a length characterizing the size either of the grains or of the pore openings

F = an unknown function.

For low values of velocity (or Reynolds number) the value of the function F has been found simply to equal its argument, so that

$$-\frac{dp}{dL} = \text{const.}\ \frac{\mu u}{\delta^2} \tag{7}$$

which is the result experimentally verified by Darcy. Flows at sufficiently high values of Reynolds number, however, are characterized by the fact that the function F is proportional to the square of its argument, so that Equation (6) takes the form

$$-\frac{dp}{dL} = \text{const.}\ \frac{\rho u^2}{\delta} \tag{8}$$

As was mentioned earlier, the pressure gradient can be accurately represented by a quadratic equation of the Forchheimer type which is valid in both the Darcy and the quasi-turbulent flow regimes. By including the length parameter δ in the unknown constants, Equations (7) and (8) can be combined into the form

$$-\frac{dp}{dL} = \alpha \mu u + \beta \rho u^2 \tag{9}$$

The two coefficients α and β defined by this equation are independent of the mechanical properties of the fluid. Since they have only the dimensions of some unknown length characterizing the structure of the porous material itself, they will henceforth be referred to as the viscous and inertial resistance coefficients of the material.

The above considerations need not be restricted to an incompressible fluid. In the case of a gas in one-dimensional steady flow through a porous medium, the mass rate of flow ρu is constant throughout the medium and may serve as an independent variable. In this case, however, effects due to changes in the momentum of the fluid cannot be ruled out a priori, and so Equation (9) must first be rewritten as a momentum equation:

$$dp + \alpha \mu u\, dL + \beta \rho u^2 dL + \rho u\, du = 0 \tag{10}$$

Introduction of the variable ρu then gives

$$\rho\, dp + \alpha \mu (\rho u)\, dL + \beta (\rho u)^2 dL + \rho (\rho u)\, du = 0 \tag{11}$$

It is convenient to replace the mass density ρ by the specific weight $\sigma = \rho g$, and the mass flow rate ρu by the weight flow rate $G = \rho u g$. With these changes, Equation (11) becomes

$$\sigma dp + \alpha \mu G dL + \beta \frac{G^2}{g} dL + \frac{G^2}{g} \sigma d\left(\frac{1}{\sigma}\right) = 0 \qquad (12)$$

If isothermal flow of a perfect gas is assumed,

$$\frac{p}{\sigma} = \frac{p_0}{\sigma_0}$$

and so

$$\frac{\sigma_0}{p_0} p dp + \alpha \mu G dL + \beta \frac{G^2}{g} dL + \frac{G^2}{g} \frac{d\left(\frac{1}{p}\right)}{\frac{1}{p}} = 0 \qquad (13)$$

Integrating over the complete path

$$\frac{\sigma_0}{p_0} \frac{p_2^2 - p_1^2}{2} + \alpha \mu G L + \beta \frac{G^2}{g} L + \frac{G^2}{g} \ln \frac{p_1}{p_2} = 0 \qquad (14)$$

or

$$\frac{p_1^2 - p_2^2}{L} = \alpha \left(\frac{2 p_0 \mu}{\sigma_0}\right) G + \left[\beta + \frac{1}{L} \ln \frac{p_1}{p_2}\right] \left(\frac{2 p_0}{\sigma_0 g}\right) G^2 \qquad (15)$$

At this point it may be noted that in the present investigation, if not in general, the momentum change term will be of negligible magnitude, and that the pressure drop equation may be written simply as

$$\frac{p_1^2 - p_2^2}{L} = \alpha \left(\frac{2 p_0 \mu}{\sigma_0}\right) G + \beta \left(\frac{2 p_0}{\sigma_0 g}\right) G^2 \qquad (16)$$

Using the perfect gas equation, this becomes

$$\frac{p_1^2 - p_2^2}{L} = \alpha (2bT\mu) G + \beta \left(2\frac{bT}{g}\right) G^2 \qquad (17)$$

where $b = R/M$.

Equation (17) will be used as the basis for correlation of the data obtained in this investigation. The purpose of the present study is to investigate the dependence of the coefficients α and β for a bed of smooth spherical particles upon the bed porosity and the specific surface. By packing the spheres in similar configurations, the porosity may be fixed while the particle size is varied. For a given sphere diameter, porosity changes will be effected by the use of different packing configurations, as will be described in Section IV.

B. Discussion of the Equation

It is interesting to compare the incompressible Forchheimer-type equation (9), which involves no assumptions as to the porosity distribution, to similar expressions for the pressure gradient obtained by writing Equation (2), due to Fair and Hatch, and Equation (3), due to Baldwinotoff and Feodoroff, as the sum of two terms with $n = 1$ and $n = 2$:

$$\text{F-H:} \quad \frac{\Delta p}{L} = \left[k S_o^2 \frac{(1-\varepsilon)^2}{\varepsilon^3}\right] \mu u + \left[k S_o \frac{(1-\varepsilon)}{\varepsilon}\right] \rho u^2 \qquad (21)$$

$$\text{B-F:} \quad \frac{\Delta p}{L} = \left[k' S_o^2 \varepsilon^{-4/3}\right] \mu u + \left[k' S_o \varepsilon^{-5/3}\right] \rho u^2 \qquad (22)$$

As was mentioned earlier, the bracketed groups corresponding to the resistance coefficients of Equation (9) prescribe two different porosity functions, with which the results of the present experiments will be compared. That the viscous term should be proportional to the square of the specific surface requires no comment. That the coefficient of the inertial term should have the dimensions (L^{-1}) may be interpreted as an expression of the fact that the acceleration experienced by the fluid particles depends upon the curvature of the streamlines. One may explain the quadratic resistance term by analogy to form drag resulting from separation as do Bakhmeteff and Feodoroff, in which case β would represent the curvature of the bed particles, or by analogy to contraction and expansion losses due to changes in the cross sectional area of the flow system, as do Chilton and Colburn (24) and Lapple (25), in which case β would represent the spacing of the constrictions. It should be realized, however, that for a granular bed these two pictures are essentially similar. A slightly different explanation of the mechanism of quadratic resistance is given by Hubbert (26) who points out that for a macroscopically parallel flow the vector sum of the inertia forces is zero, so their effect in impeding the fluid motion can only be indirect. Hubbert's picture of the quadratic resistance is that "the distortion of the flow lines by the inertia forces in the fluid increases the local velocity gradients, which in turn increase the frictional forces over what they would have been for the same rate of flow had the distortion not occurred". In this regime the resistance

to flow would still be attributable to viscous stresses, or stresses arising from momentum transfer by molecular agencies. At sufficiently high values of Reynolds number, presumably, a truly turbulent regime must eventually be reached, in which the resistance is lodged in stresses arising from transfer of momentum on a macroscopic scale. Since these two effects are both proportional to the square of the fluid velocity, their relative contributions cannot be appraised, but they may nevertheless be grouped together under the collective title of "inertial resistance".

IV EXPERIMENTAL EQUIPMENT

A. The Sphere Bed

Steel ball bearings served as the particles for the beds studied in the present investigation. Bearings of 0.125, 0.250, 0.500, and 0.875-inch diameter were used. Variations in porosity were obtained by packing the beds* according to the configurations shown diagrammatically in Figure 2. Cubic and hexagonal modes of packing provided the maximum and minimum limits, respectively, of the bed porosity obtainable with spherical particles. Since it was desired to have some intermediate porosities, a random packing was included, even though it necessarily involved some wall effects. In addition, a mixed mode consisting of alternate layers of cubic and hexagonal packing was used. Although the non-uniform porosity distribution of this "stratified" packing could be expected to affect the measured values of α and β, it was hoped that the ratio of the two might be unaffected. The experimental data later tended to justify this belief.

Since it was essential to observe the bed in order to prevent mistakes during packing, the flow tube, 28 inches in length, was fabricated from 1-inch Lucite sheet, with 0.03-inch Neoprene sheet serving as a gasket between the bolted sections. A square cross section 3.5 inches wide simplified the wall insert problem by permitting an integral number of spheres in each layer in order to

*For reasons given later, only the 0.250-inch diameter bearings were packed in each of the above modes.

minimize the non-uniform porosity distribution at the walls.

The method of systematically packing the spheres into the tube can be seen from Figure 3. By supporting the bed upon the top of a threaded rod and the tube upon a disk travelling on this rod, the tube could be raised around the bed, thus permitting all the loading operations to be conducted at the top of the tube. A top view of the array of 0.125-inch spheres during the loading procedure is given in Figure 4. Once packed, the beds were rigidly constrained by end sections employing 16 gage wire screen supported by a perforated metal plate. The details of the plate and screen can be seen in Figure 5.

B. Insert Design

In the earlier discussion of the wall effect, it was noted that errors due to the non-uniform distribution of porosity along the wall were less susceptible to rational correction in the regime of inertial resistance than in the Darcy zone, and that mitigation of these errors might be realized by filling the voids at the wall in the case of the systematic packings. Since inertial effects depend upon the curvature of the streamlines, it was desired that the wall inserts not only fill the voids, but simulate the shape of the bed particles as closely as possible. It was felt impractical to fill the voids with half spheres, but in the two worst cases (the 0.375- and 0.500-inch sphere beds) a reasonable compromise was reached by the use of inserts fashioned from half-round brass rod in such a manner that only the rounded side of the rod was exposed to the flow. Figure 6 shows layers

of 0.875-inch bearings with an insert of this type. For the smaller spheres, no half-round material was available, and so the inserts were made from round rod. For these two cases, however, the wall effect is of reduced importance due to the large ratio of tube width to ball diameter.

C. Measuring Equipment

The experiments were performed with nitrogen gas as the working fluid. The procedure consisted of determining the pressure and temperature at both ends of the granular bed as a function of the rate of flow through the bed. Since difference between the inlet and outlet pressures were often small, the inlet and outlet pressures were measured with mercury manometers, while the pressure drop across the bed was measured with a water manometer or one of two draft gages, depending upon its magnitude. The manometer system used for these measurements is shown in Figure 7. The gas temperatures were measured with mercury thermometers.

The measurements of gas flow rate were made with the equipment used at the Jet Propulsion Laboratory for routine permeability testing of porous metal specimens. This equipment, shown in Figure 8, utilized four Fisher-Porter Flowrators in parallel to measure gas flow rates up to 100 cu ft/min. The gas pressure was controlled by three Grove regulators, also in parallel. For the sphere bed measurements, the flow was diverted through the packed column and back into the Flowrator system.

Figure 9 shows all the equipment assembled with the flow tube

(encased in a supporting plywood frame for additional strength) in a horizontal position. In two cases, however, the tests were made with the tube in a vertical position. This was required to lessen the possibility of collapse of the highly unstable cubic packing of 0.250-inch spheres, and to prevent channeling of the random packing of the same spheres.

A cross section of the flow tube with the entrance and exit sections in position is shown in Figure 10. The unconventional location of the upstream pressure tap was selected because the dynamic pressure picked up at that region was found to be less than that at any other available point. Both pressure taps (orifice diameter 0.063 inch) were originally located on the cylindrical portions of the entrance and exit sections, but it was found that the eddies generated by the ring supporting the felt diffusing disk introduced a fluctuating dynamic pressure of such a large magnitude that the upstream tap had to be moved to the location described above.

In the calibration of the end section it was desired to correct only for the dynamic pressure picked up and for the pressure drop through the supporting screens, and not to include the pressure drop due to friction along the tube wall. Consequently a special calibration tube of sheet brass was made with a length just sufficient to give a 1/4-inch separation between the supporting screens when the end sections were fastened in place. The pressure drop across this system, calibrated as a function of weight flow rate, was used to correct the readings obtained with the packed tube. This cali-

bration process was repeated with another tube for the cases where a shorter bed was used in conjunction with an additional inserted bed support and an additional wire screen.

D. Temperature Correction

The equation with which the data from the present experiment were correlated was based upon the assumption of isothermal flow. At high rates of flow this condition could not be maintained, but the maximum deviation of the inlet and outlet absolute temperatures from the average temperature was about two per cent, and this error is considered negligible. Although the gas temperature was thus approximately constant across the bed, however, it varied with the rate of flow. Since the nitrogen used in this experiment was throttled through regulators from a pressure of about 2000 psig. in the storage cylinders to less than 25 psig. in the bed, the gas temperature varied from a maximum of about 80°F at low flow rates to a minimum of about 25°F at the highest flow rates. This large difference made it necessary to modify Equation (17) by using two values of temperature, T_α and T_β, corresponding to the temperatures obtaining in the bed over the regions in which the coefficients α and β were defined.

V PROCEDURE AND RESULTS

A. Agreement of Experimental Curves with the Quadratic Equation

The first series of tests was made with each of the four sphere sizes arranged in Packing A, the hexagonal array of minimum porosity. Table 1 summarizes the geometrical properties of these packings. The results of these tests are presented in Figure 11 in terms of the difference between the squares of the inlet and outlet absolute pressures divided by the length of the bed (henceforth called the pressure-square gradient) as a function of the weight rate of flow through the bed. From these data and from knowledge of the temperature and viscosity, the viscous resistance coefficient α was determined by fitting a straight line of slope 1 to the points lying in the Darcy regime. The inertial resistance coefficient β might have been determined most accurately by fitting a quadratic curve to the data according to the method of least squares, but it was felt that the precision of the data did not justify such an elaborate procedure. Since the best curves drawn through the experimental points either attained or closely approximated a slope of 2 at their upper ends, it was found convenient to extend slightly the curves which fell short until a slope of 2 was reached and to extrapolate the lines of this slope to a point where the contribution of the linear term was negligible and β could be calculated directly. The values of α and β determined by the above procedure (summarized in Table II) were then used to compute the solid curves of Figure 11.

It may be seen that the agreement between the calculated curves

and the experimental points is less satisfactory in the case of the two largest ball sizes than for the smaller balls. The poor fit is attributed to uncertainty in the values of α obtained with the larger spheres as a result of scatter in reading very small pressures (of the order of 0.001 inch of water) on the low range draft gage. For this reason it was felt that the values of α given by these spheres in the higher porosity packings would not be reliable, and that the tests with varying porosity would have to be performed with the smaller spheres. On the other hand, it had been found that the task of systematically packing the 0.125-inch bearings in any mode other than the stable hexagonal array was impossible. Consequently, the 0.250-inch bearings were the only ones which could be used to realize the porosity variations.

Another conclusion that can be drawn from Figure 11 is that the ratio of tube width to sphere diameter in the case of the two largest ball sizes is too small to allow elimination of the wall effect in the inertial regime, even with the use of inserts to fill the voids at the wall. This fact is evidenced by the abnormally wide separation of the two lower curves in the slope 2 region. The spacing of the curves given by the two smaller spheres, on the other hand, is that predicted by the theory. Support was thus given to the belief that the wall effect inherent in the random packing would be of minor importance in the case of the 0.250-inch spheres owing to the large ratio of tube-to-ball size.

B. Comparison of Results with the Two Theories

The pressure-square gradient vs weight flow rate curves obtained with the 0.25-inch spheres in various modes of packing are presented in Figure 12. It may be noted that the experimental curve given by the cubic packing breaks upward more sharply than do the calculated curves or the other experimental curves. This behavior is understandable, since unlike the other modes the cubic array contains straight, uninterrupted channels in which a flow transition similar to that observed in rough pipes would be expected. By the same reasoning it might be anticipated that the cubic mode would exhibit an inertial resistance somewhat lower than would be expected upon the basis of porosity alone, and this was later found to be the case.

The values of α , β , and β/α for the 0.25-inch spheres given in Table II are plotted versus porosity in Figure 13. As had been hoped, the value of β/α for the mixed mode of packing B was consistent with the other modes, even though the values of α and β individually were higher than normal as a result of non-uniform porosity distribution. In contrast to the behavior of α and β , it may be seen that β/α appears to be approximately independent of porosity, a result which was not anticipated. In order to compare the viscous coefficients of Figure 13 with the conflicting resistance functions of Dakhnoteff-Feodoroff and Kozeny (or Fair-Hatch), the curves of Figure 1 and the points of Figure 13 are presented in Figure 14 in terms of the dimensionless ratios

$$\frac{f(\varepsilon)}{f(39.2)} \quad \text{and} \quad \frac{\alpha(\varepsilon)}{\alpha(39.2)}$$

since the expressions coincide at a porosity of about 39.2 per cent. Although the agreement is not exact, it is apparent that the experimental points tend to fall in along the Kozeny curve. From this result it is concluded that the equation of Kozeny or Fair-Hatch expresses the variation of the viscous resistance coefficient more correctly than does that of Bakhmeteff and Feodoroff. Reference to Equations (21) and (22), however, shows that both expressions failed to predict the results of Figure 13, which indicates that the influence of porosity upon the resistance to flow was approximately the same in both the viscous and inertial regimes.

In order to investigate the dependence of the viscous resistance coefficient upon the specific surface of the beds, the Kozeny porosity function was used to correct the value of α calculated from the curves of Figure 11 to a porosity of 27 per cent. The values, when plotted versus specific surface in Figure 15 show that α is proportional to S_o^2, as was expected from the dimensional considerations. Because of the wall effect in the inertial regime attending the hexagonal packing of the two largest sphere sets mentioned earlier, the results of Figure 11 could not be used to investigate the variation of the inertial resistance coefficient with specific surface. For this purpose the pressure-square gradient vs flow rate curves obtained from the spheres in cubic arrays were compared in Figure 16. Even though the contribution of the tube wall area to the total bed surface is considerable in these packings, the cubic mode automatically eliminates the uneven porosity distribution at the boundaries of the bed, thus mitigating the wall effect as much as possible for a given particle size. The values of β yielded by the cubic beds are

included in Figure 15 as functions of S_o. Although the agreement with the predicted behavior is less convincing than was the case with the viscous coefficient, a direct linear relationship between β and the specific surface seems apparent.

C. Extension of the Kozeny Equation to the Inertial Regime

Although the data obtained in the present investigation were not numerous enough to justify the determination of the constant required for an independent empirical equation for pressure drop, the relationship between the pertinent variables described above seemed convincing enough to permit at least an extension of the Kozeny equation to the regime of inertial or quasi-turbulent resistance by the addition of a quadratic term . From Figure 13 it was seen that the ratio β/α was approximately independent of the bed porosity, a result not predicted by either of the Equations (21) and (22). Simply on dimensional grounds, however, the ratio would be expected to vary inversely with the specific surface of the bed. When the data obtained from the 0.125-inch and 0.250-inch bearings (the most reliable because of the negligible wall effect) were plotted in Figure 17, it was found that the best fit was obtained by the linear relation

$$\beta/\alpha = \frac{0.064}{S_o}$$

If the Kozeny equation is accepted as valid in the viscous regime, this evaluation of the ratio β/α fixes the value of the empirical dimensionless constant of the quadratic resistance term, and the

complete equation expressing the pressure drop across a bed of smooth spherical particles as a function of the fluid properties, the characteristics of the bed, and the rate of flow may be written as

$$\frac{\Delta p^2}{L} = 10 S_o^2 \frac{(1-\varepsilon)^2}{\varepsilon^3} bT\mu G + 0.64 S_o \frac{(1-\varepsilon)^2}{\varepsilon^3} \frac{bT}{g} G^2 \qquad (23)$$

It is of interest to compare this equation with experimental data on flow through sphere beds published by other investigators. Two sets of such data immediately available to the author were obtained by Muskat and Botset (27) from the flow of air through small glass beads and by Chalmers, Taliaferro, and Rawlins (18) from the flow of natural gas through lead shot. Correction for the appreciable deviation of natural gas from the perfect gas behavior postulated in the preceding development was realized by modifying Equation (23) to include an average value of the compressibility factor $Z = p/\sigma bT$. Figure 18 presents the experimental data taken from the above references and the theoretical curves calculated from Equation (23). Considering the uncertainties in the specific surface of the beds (taken as $6/d$) due to the unknown eccentricity, roughness, and size variation of the small particles (especially the smallest size of graded shot) the agreement appears good.

VI THE REYNOLDS NUMBER OF A POROUS MATERIAL

In Section II it was mentioned that the quadratic equation of the Forcheimer type might possibly permit definition of the Reynolds number of a flow through a complex porous material, even if the length parameter characterizing the material is not readily measurable. Since the Reynolds number of a flow system represents the ratio of the inertia forces to the viscous forces, it seems legitimate (at least in the case of laminar flow) to assume that this ratio is the same as that of the quadratic resistance term of a two-term Forcheimer-type equation to the linear term. Using Equation (17) in this fashion, the Reynolds number may be written

$$Re = \frac{\beta G}{\alpha \mu g} \tag{24}$$

and it may be seen that the unknown length entering into the Reynolds number expression is β/α, the ratio of the inertial and viscous resistance coefficients. Equation (17) can also be used to define a friction factor as

$$C_f = \frac{1}{\beta} \frac{\Delta p^2}{L} \frac{g}{2 b T G^2} \tag{25}$$

$$= 2 \quad \text{in inertial regime}$$

$$= \frac{2}{Re} \quad \text{in Darcy regime}$$

Over the entire range of flows, then,

$$C_f = \frac{2}{Re} + 2 \tag{26}$$

Since this relation was derived from a two-term quadratic pressure gradient expression of the Forcheimer type, any data which fit such a quadratic equation will fit Equation (26). As an example some typical data obtained from the sphere bed experiments are presented in Figure 19.

It may be noted that the above correlation is so general that it may also be said that there is little value in a method of correlation which requires two characteristic length parameters (α and β) when it is well known that data on flow through sphere beds can be correlated with only one length parameter, the sphere diameter. Such a statement, however, emphasizes the main point of the development presented above: in general a porous material can only be completely characterized by both of the length parameters defined by the two-term quadratic resistance equation. This type of representation is the only one which can be applied to complex consolidated materials such as porous metals, since it can correlate the behavior of specimens whose pressure gradient vs. flow rate curves intersect or cross one another. Such behavior is often encountered in porous metals, since the inertial resistance coefficient is apparently more sensitive to sintering conditions than is the viscous coefficient. Intersecting curves of this type have also been obtained in tests upon consolidated sands (28).

It may thus be seen that from the general point of view a sphere bed is a special case in which correlation on the basis of one length

parameter alone is possible only because of the geometrical simplicity of the porous structure. The experimental data of Figure 15 reveal that the reason for this is that

$$\alpha \sim S_o^2 \sim 1/\delta^2$$

$$\beta \sim S_o \sim 1/\delta$$

Thus both β/α and $1/\beta$ are directly proportional to the sphere diameter. Application of this proportionality to the Reynolds number and friction factor expressions restores their familiar appearance.

The conditions necessary for the validity of the assumption leading to Equation (24) are not obvious at the present time. Certainly the condition of laminar flow is sufficient, but the state of flow obtaining in a porous medium cannot be readily ascertained. Although the writer cannot conceive the existence of fully developed turbulence within the minute interstices of a material such as a porous metal, the existence of stationary vortices and eddies is not unlikely. Under such conditions the energy dissipation would still result from momentum transfer on a molecular scale. On the other hand it may be observed from the data of the present experiment that the Reynolds number assumption is apparently valid for porous structures as coarse as the gross array of 0.875-inch spheres, in which turbulent conditions almost certainly obtain at high rates of flow. Consequently it appears that the validity of Equation (24) does not depend upon a certain state of flow, but requires only a flow transition smooth enough that the pressure drop data follow a quadratic curve of the Forcheimer type.

VII CONCLUSIONS

1. The present experiment provides support for Forcheimer's conclusion that the pressure gradient attending fluid flow through a porous medium can be accurately expressed as a function of flow rate by a simple quadratic equation. Such an equation defines two length parameters characteristic of the porous structure. The parameter by which the linear term is multiplied (dimensions $[L^{-2}]$) is the inverse of the permeability coefficient defined by Darcy's law, and is called the "viscous resistance coefficient". The multiplier of the quadratic term (dimensions $[L^{-1}]$) is called the "inertial resistance coefficient".

2. The influence of porosity upon the resistance of a bed of smooth spherical particles to fluid flow in the Darcy regime is expressed more accurately by the Kozeny (or Fair-Hatch) equation than by the equation of Bakhmeteff and Feodoroff.

3. Contrary to both the Fair-Hatch and Bakhmeteff-Feodoroff expressions, the influence of porosity in the inertial or quasi-turbulent regime was found to be approximately the same as in the viscous range.

4. The influence of the specific surface of the bed upon the linear and quadratic resistance terms is predicted correctly by the equations of Fair-Hatch and Bakhmeteff-Feodoroff. This special functional dependence of the viscous and inertial resistance coefficients upon the specific surface is responsible for the fact that sphere bed data can be correlated with the use of only one length parameter.

NOMENCLATURE

A	Cross-sectional area of a hypothetical capillary tube
a	A constant
b	A constant Perfect gas constant, $[L\theta^{-1}]$
C_f	Friction factor (dimensionless)
D	Width of flow channel $[L]$
d	Derivative notation
F	A function
f	A function.
G	Weight flow rate/unit area $[ML^{-1}T^{-3}]$
g	Acceleration due to gravity $[LT^{-2}]$
k	A constant
L	A length variable
m	Equivalent hydraulic radius $[L]$
n	A number
P	Pressure $[ML^{-1}T^{-2}]$
S	Surface area of porous material per unit total volume of material $[L^{-1}]$
S_o	Surface area of porous material per unit solid volume of material $[L^{-1}]$
T	Absolute temperature $[\theta]$
u	Fluid velocity $[LT^{-1}]$
Z	Compressibility factor (dimensionless)
α	Viscous resistance coefficient $[L^{-2}]$

β Inertial resistance coefficient $[L^{-1}]$

δ A length parameter $[L]$

ε Porosity (dimensionless)

θ Dimension of temperature

μ Dynamic viscosity $[ML^{-1}T^{-1}]$

ρ Fluid density $[ML^{-3}]$

σ Specific weight $[ML^{-2}T^{-2}]$

τ Shearing stress $[ML^{-1}T^{-2}]$

REFERENCES

1. Dawes and Wheeler, Jour. Aero. Sci., 15, 509 (1948).

2. Dawes and Martens, AIME Tech. Pub. No. 2343, Met. Tech., 1948.

3. Darcy, H. P. G., "Les Fontaines Publiques de la Ville de Dijon" Victor Delmont, Paris, 1856.

4. Dupuit, A. J. E. J., "Etudes Theoretiques et Pratiques sur le Mouvement des Eaux", 1863.

5. Kozeny, Ber. Wien. Akad. 136, 271 (1927).

6. Fair, G. M. and Hatch, L. P., "Fundamental Factors Governing the Streamline Flow of Water through Sand", J. Am. Water Works Assoc. 25, 1551 (1933).

7. Carman, P. C., "Fluid Flow through Granular Beds", Tr. Inst. Ch. Engs., 15, 150 (1937).

8. Carman, P. C., "The Determination of the Specific Surface of Powder", I Journ. Soc. Chem. Indust. 57, 225 (1938).

9. Hatch, L. P., Discussion of paper "Flow through Granular Media" J. App. Mech., Trans ASME, 60, A-86 (1938).

10. Hatch, L. P., "Flow through Granular Media", J. App. Mech., Trans. ASME, 62, A-109 (1940).

11. Hatch, L. P., "Flow of Fluids through Granular Materials: Filtration, Expansion, and Hindered Settling", Trans. Am. Geophys. Union, p. 536, 1943.

12. Bakhmeteff, B. A., and Feodoroff, N. V., "Flow through Granular Media", J. App. Mech., Trans. ASME, 59, A-97 (1937).

13. Bakhmeteff, B. A. and Feodoroff, N. V., "Flow through Granular Media", Proc. of Fifth Int. Cong. for Appl. Mech., 1937.

14. Bakhmeteff, B. A. and Feodoroff, N. V., discussion of paper "Flow through Granular Media", J. App. Mech., Trans. ASME, 60, A-86 (1938).

15. Bakhmeteff, B. A. and Feodoroff, N. V., Discussion "Flow of Fluids through Granular Materials: Filtration, Expansion, and Hindered Settling", Trans. Am. Geophys. Union, p. 536, 1943.

16. Carman, P. C., "Fundamental Principles of Industrial Filtrations" Trans. Ind. of Ch. Engs., 16, 168 (1938).

17. Forcheimer, P., Zeit. VDI., 45, 1781 (1901).

18. Chalmers, Taliaferro, Rawlins, Trans. Amer. Inst. Min. Metall. Eng., Pet. Div., 98, 375 (1932).

19. Ruth, B. F., Industrial and Eng. Chem. 38, 546 (1946).

20. Furnas, C. C., Bull. U. S. Bur. Min. No. 307 (1929).

21. Gretton and Fraser, J. Geol., 43, 785 (1935).

22. Rose, H. E., Inst. of Mech. Engrs., App. Mech. Proc., 153, 141 (1945).

23. Muskat, M., "Flow of Homogeneous Fluids Through Porous Media", McGraw-Hill, 1937.

24. Chilton and Colburn, Trans. Amer. Inst. Chem. Engrs., 26, 178 (1931).

25. Lapple, C. E., Commentary on a paper by Brownell and Katz, Chem. Eng. Prog., 43, 537 (1947).

26. Hubbert, M. K., Sixth Int. Cong. App. Mech., (1946).

27. Muskat and Botset, Physics, 1, 27 (1931).

28. Johnson and Taliaferro, TP 592, U. S. Bur. Min. (1938).

TABLE I

Geometric Properties of Sphere Beds

Bed Number	1	2	3	4	5	6	7	8	9
Packing Type	A	A	B	C	D	A	D	A	D
Sphere Diameter d (in.)	0.125	0.250	0.250	0.250	0.250	0.500	0.500	0.875	0.875
Bed Length L (in.)	17.1	24.0	23.9	24.0	16.5	24.2	24.0	24.1	24.5
L/d	137	96	95.8	96	66	48.4	48	27.6	28
D/d (D = tube width, in.)	28	14	14	14	14	7	7	4	4
Description of Insert Rod Material	1/16 round	1/8 round	1/8 round	none	none	3/8 half round	none	5/8 half round	none
Bed Volume (in.^{3})	210	295	294	295	203	297	295	296	301
Sphere Volume (in.^{3})	149	203	184	178	106	189	154	172	157
Insert Volume (in.^{3})	4.1	11.7	6.9	0	0	24.7	0	37.4	0
Total Packing Volume (in.^{3})	153	215	191	178	106	214	154	210	157
$\frac{\text{Insert Volume}}{\text{Packing Volume}}$ (percent)	2.7	5.4	3.6	0	0	11.6	0	17.9	0
Bed Porosity (percent)	27.1	27.0	35.2	39.7	47.8	28.0	47.8	29.2	47.8
Missing Sphere Volume - Insert Volume (in.^{3})	1.3	3.3	2.0	-	0	4.2	0	9.2	0
$\frac{\text{Missing Sphere Volume - Insert Volume}}{\text{Packing Volume}}$ (percent)	0.8	1.5	1.0	-	0	2.0	0	4.4	0
Exposed Surface Area of Tube (in.^{2})	239	336	335	336	231	160	336	171	343
Exposed Surface Area of Inserts (in.^{2})	264	374	240	0	0	264	0	239	0
Surface Area of Spheres (in.^{2})	7170	4880	4410	4260	2540	2272	1850	1180	1078
Surface Area of Packing (in.^{2})	7434	5254	4650	4260	2540	2536	1850	1419	1078
Nominal Surface Area of Packing with Ideal Packing at Walls (in.^{2})	7440	5240	4620	-	2540	2620	1850	1500	1078
Difference in Packing Surface due to Inserts (percent)	-0.1	+0.3	+0.6	-	0	-3.2	0	-5.4	0
Total Bed Surface (Tube Included) (in.^{2})	7673	5590	4985	4596	2771	2696	2186	1590	1421
$\frac{\text{Surface Area of Inserts}}{\text{Bed Surface Area}}$ (percent)	3.4	6.7	5.2	0	0	9.8	0	15.0	0
$\frac{\text{Surface Area of Tube}}{\text{Bed Surface Area}}$ (percent)	3.1	6.0	7.2	7.3	8.3	5.9	15.4	10.8	24.1
Specific Surface $S_o = \frac{\text{Bed Surface Area}}{\text{Packing Volume}}$ (in.$^{-1}$)	50.0	26.0	26.1	25.8	26.1	12.6	14.2	7.59	9.05

TABLE II

Summary of Sphere Bed Data

Bed Number	Porosity (ε)	S_o (in.$^{-1}$)	T_α (°F)	T_β (°F)	α (in.$^{-2}$)	β (in.$^{-1}$)	β/α (in.)
1	27.1	50.0	56	30	3.28×10^{5}	4.21×10^{2}	1.28×10^{-3}
2	27.0	26.0	59	46	8.19×10^{4}	2.07×10^{2}	2.53×10^{-3}
3	35.2	26.1	55	35	5.20×10^{4}	1.28×10^{2}	2.46×10^{-3}
4	39.7	25.8	70	63	2.25×10^{4}	6.11×10^{1}	2.71×10^{-3}
5	47.3	26.1	78	65	7.31×10^{3}	1.64×10^{1}	2.24×10^{-3}
6	28.0	12.6	63	43	1.66×10^{4}	7.06×10^{1}	4.25×10^{-3}
7	47.8	14.2	-	42	-	9.94	-
8	29.2	7.59	63	33	5.46×10^{3}	2.69×10^{1}	4.93×10^{-3}
9	47.3	9.05	-	29	-	5.49	-

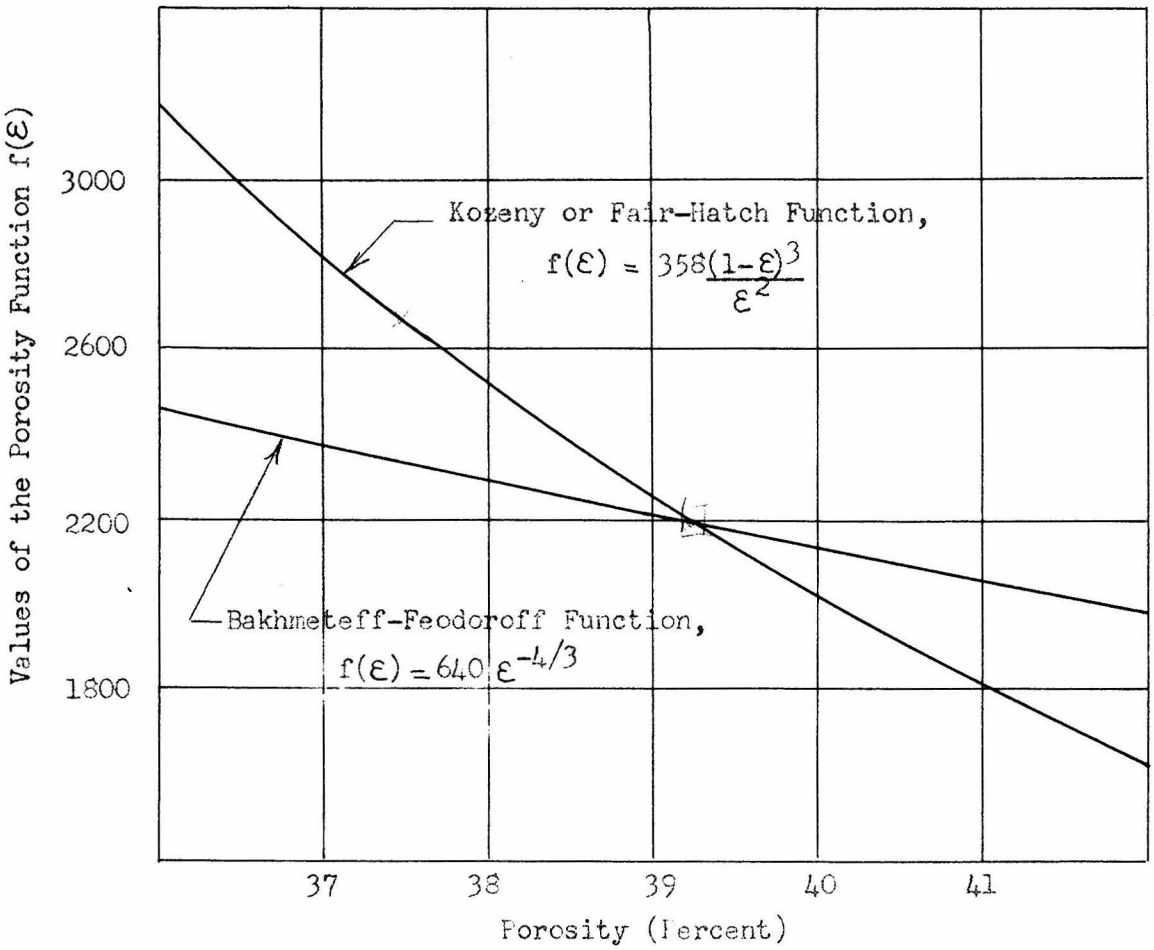

Fig. 1

Graphs of the conflicting porosity functions given by Bakhmeteff and Feodoroff, and by Kozeny or Fair and Hatch.

Packing Type Designation	Description	Schematic Representation
A	Hexagonal	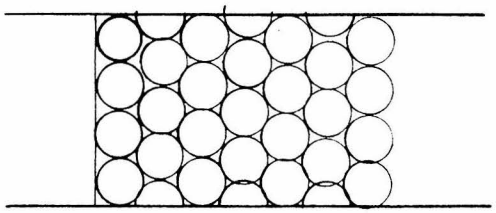
B	Mixed hexagonal and cubic	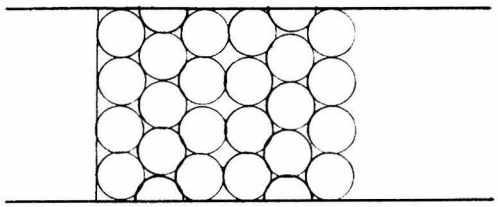
C	Random	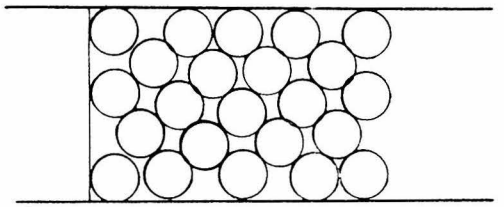
D	Cubic	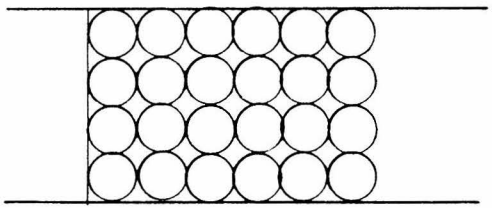

Fig. 2 Identification of the modes of sphere packing

Fig. 3

Illustration of Loading Procedure

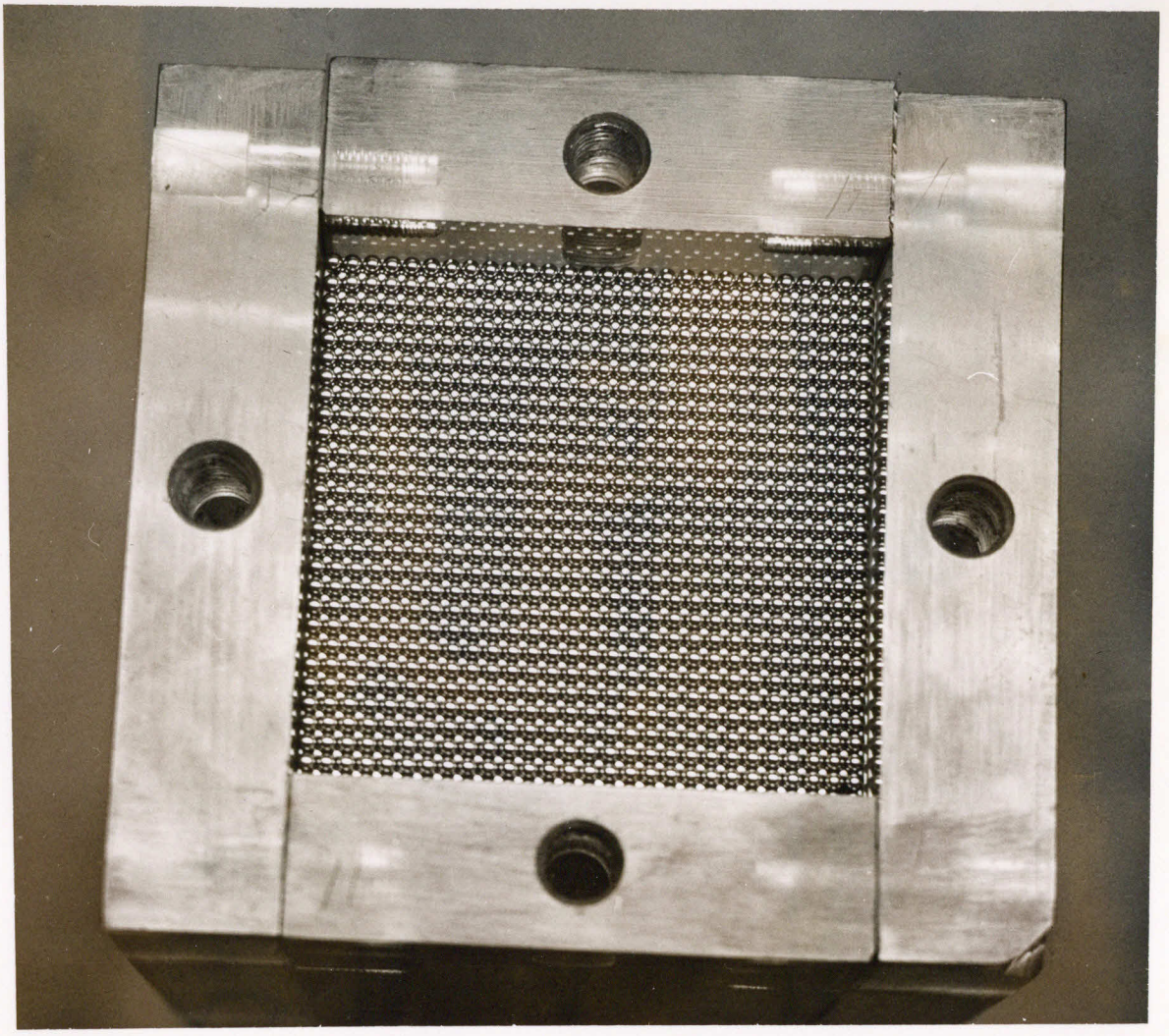

Fig. 4

Top View of Column Packed with 0.125-in. Spheres in Packing A

Fig. 5

View Showing Details of Bed Support Plate

Fig. 6

View Showing Type of Insert Used with 0.875-in. Spheres

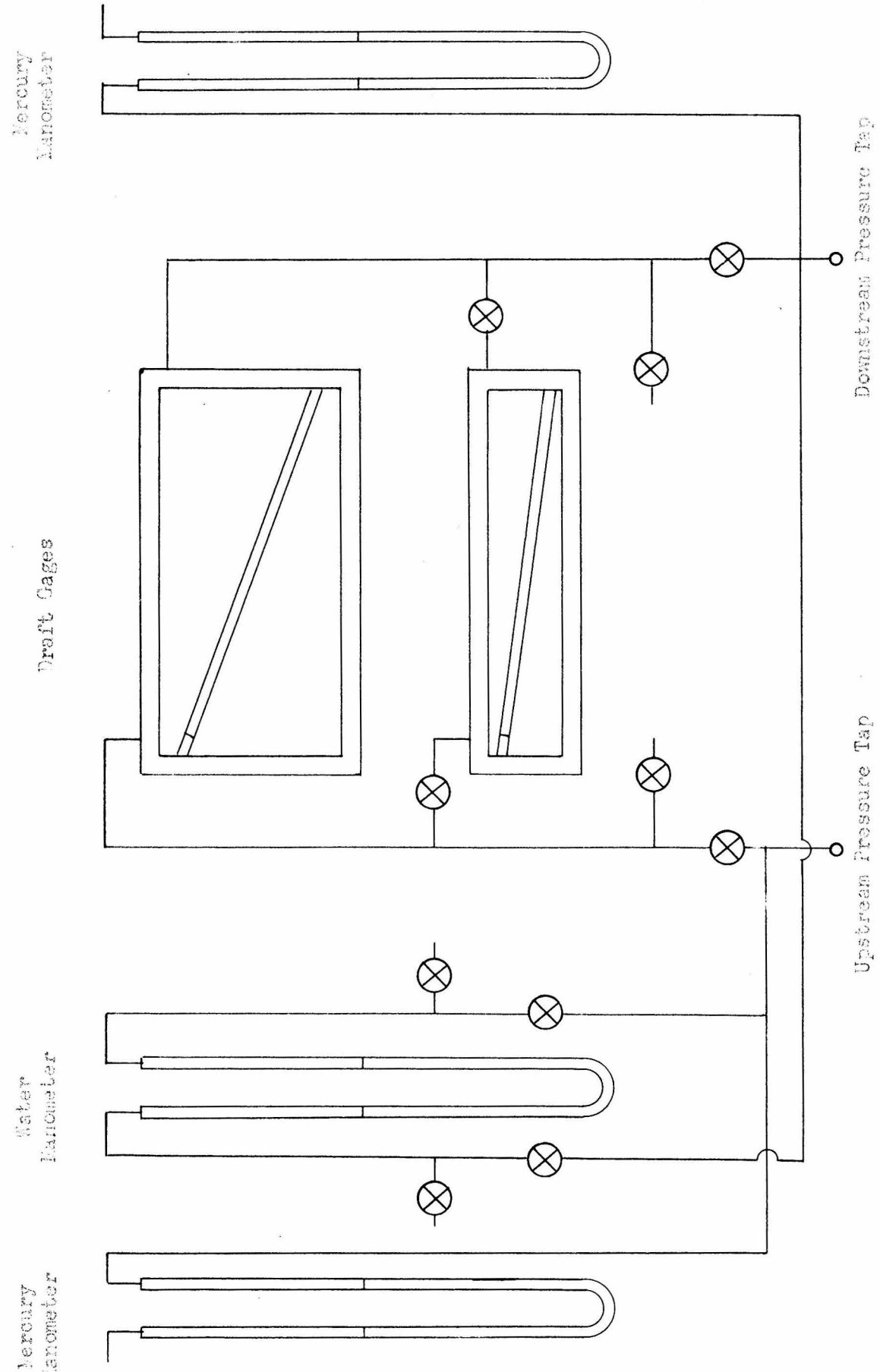

Fig. 7 Schematic Diagram of Manometer System

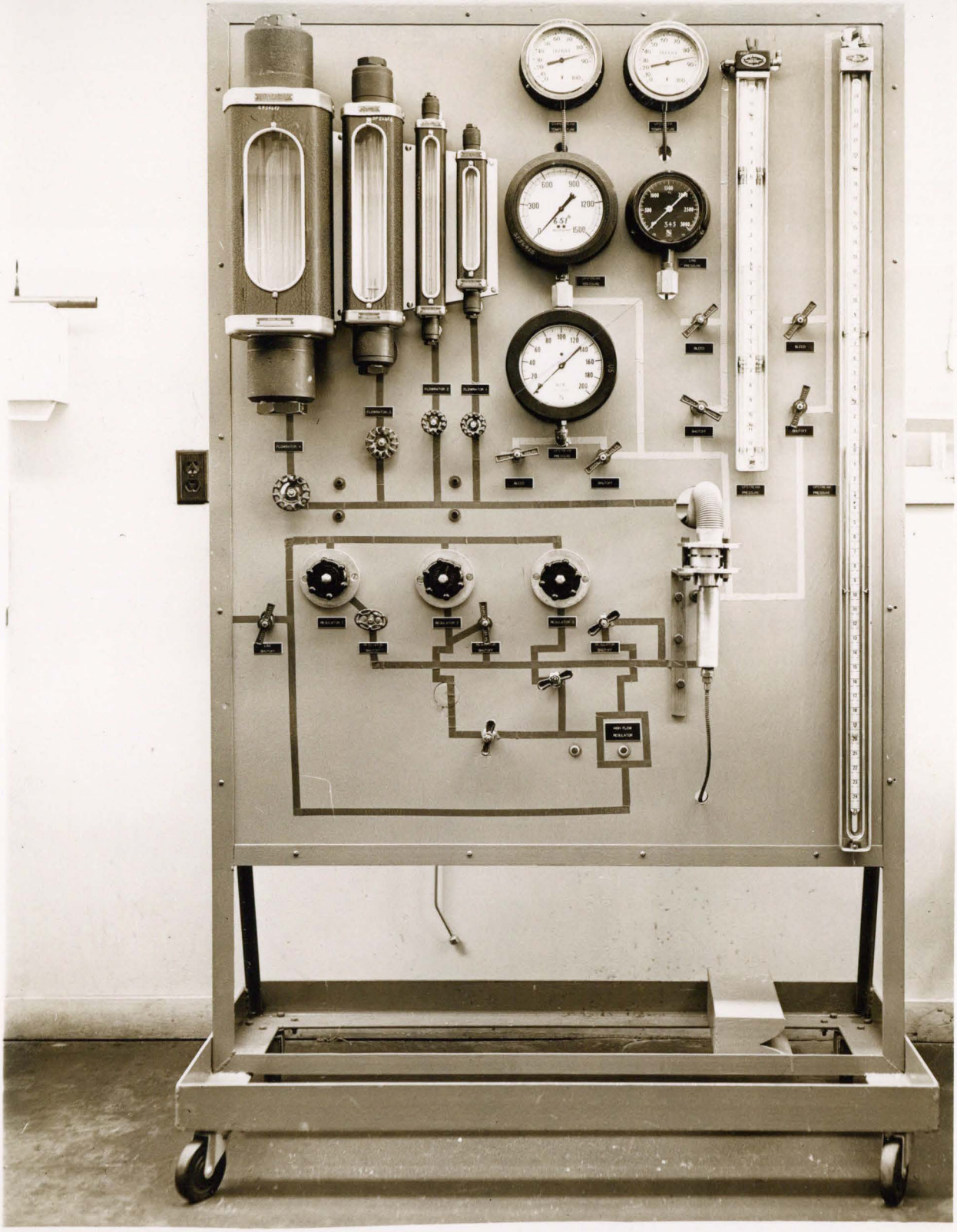

Fig. 8

Equipment for Routine Permeability Testing of Porous Metals.

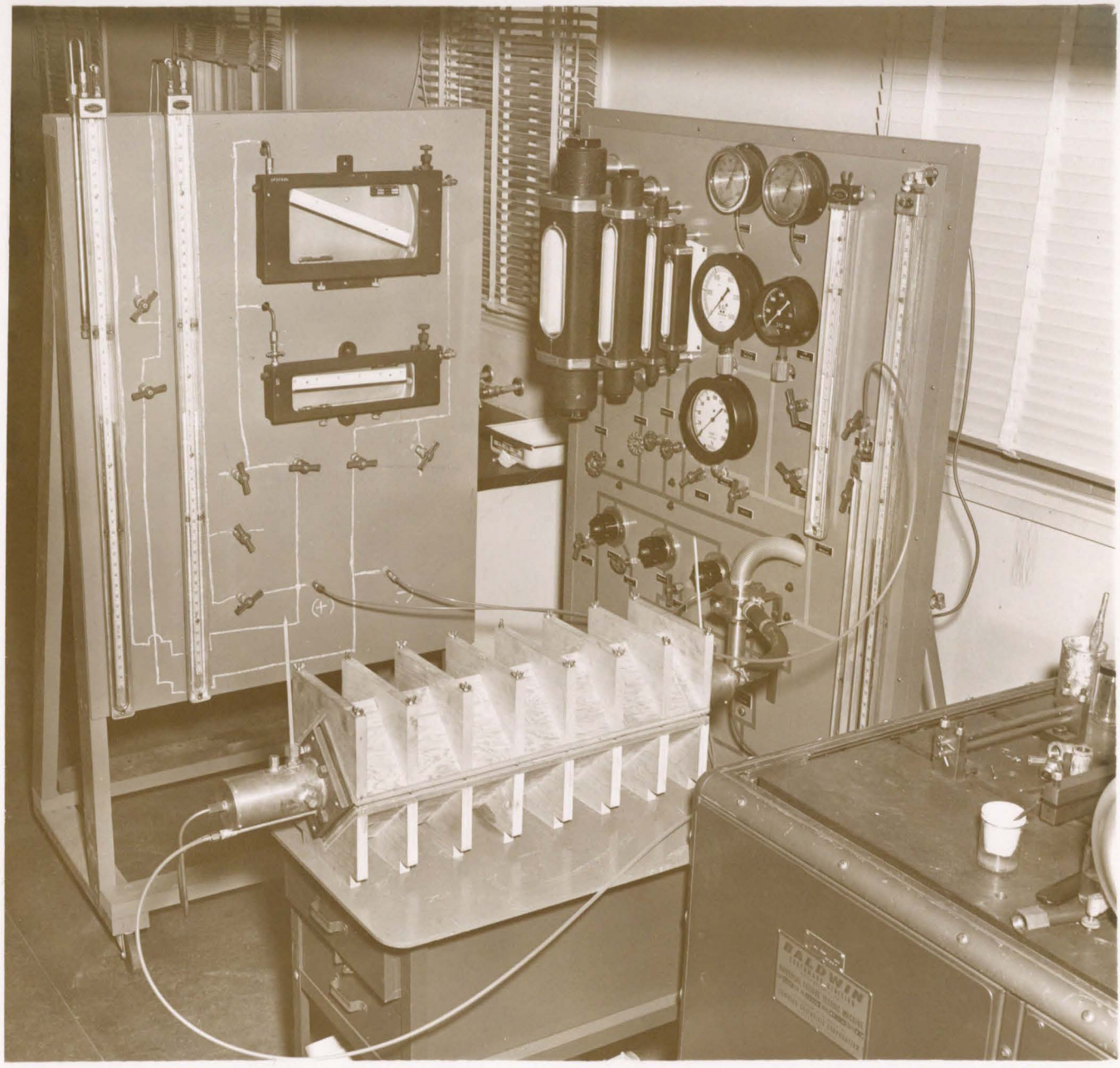

Fig. 9

Assembly of Flow Tube, Manometer Panel, and Flow Measuring Equipment

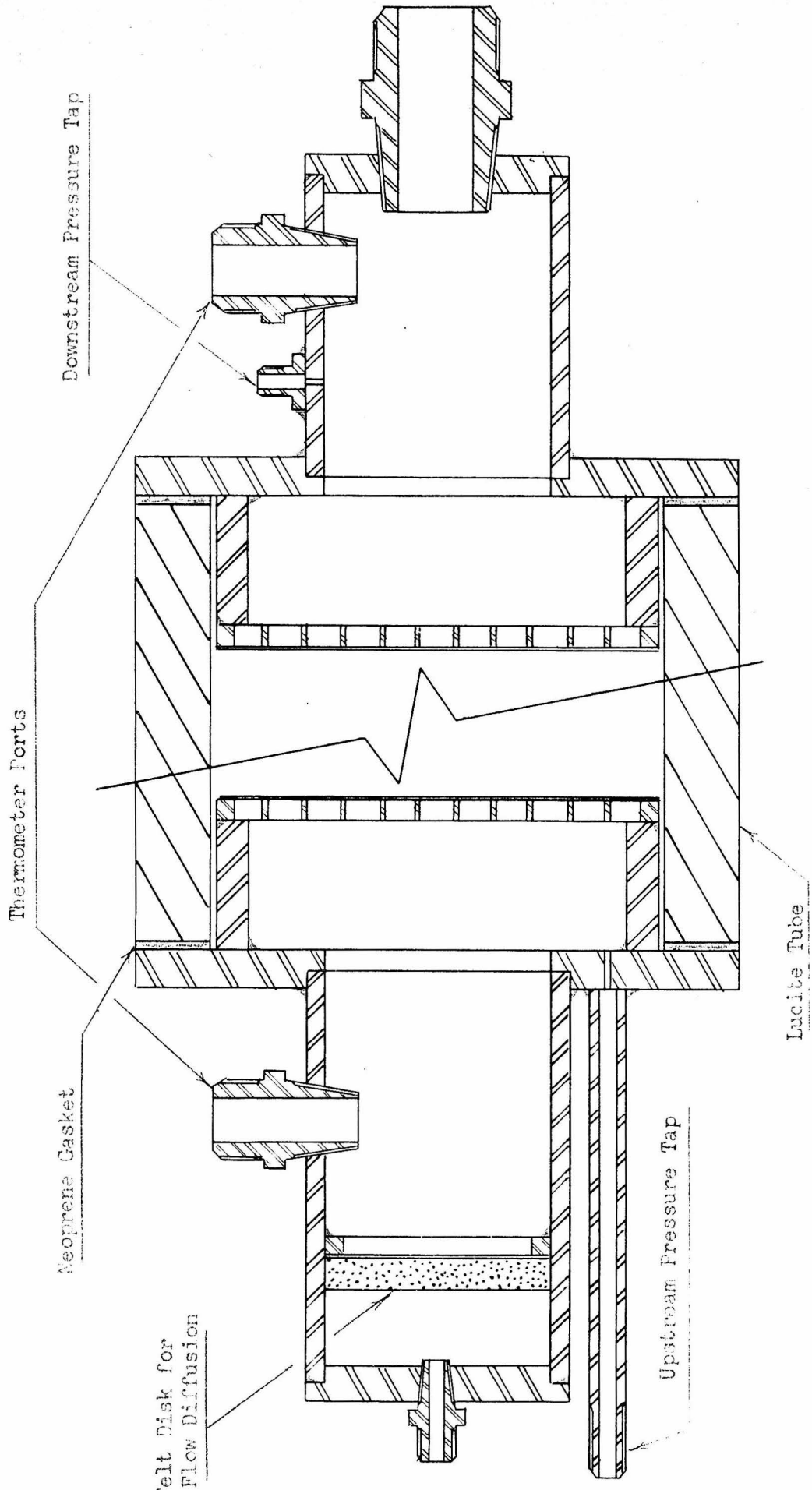

Fig. 10 Cross Section of Flow Tube

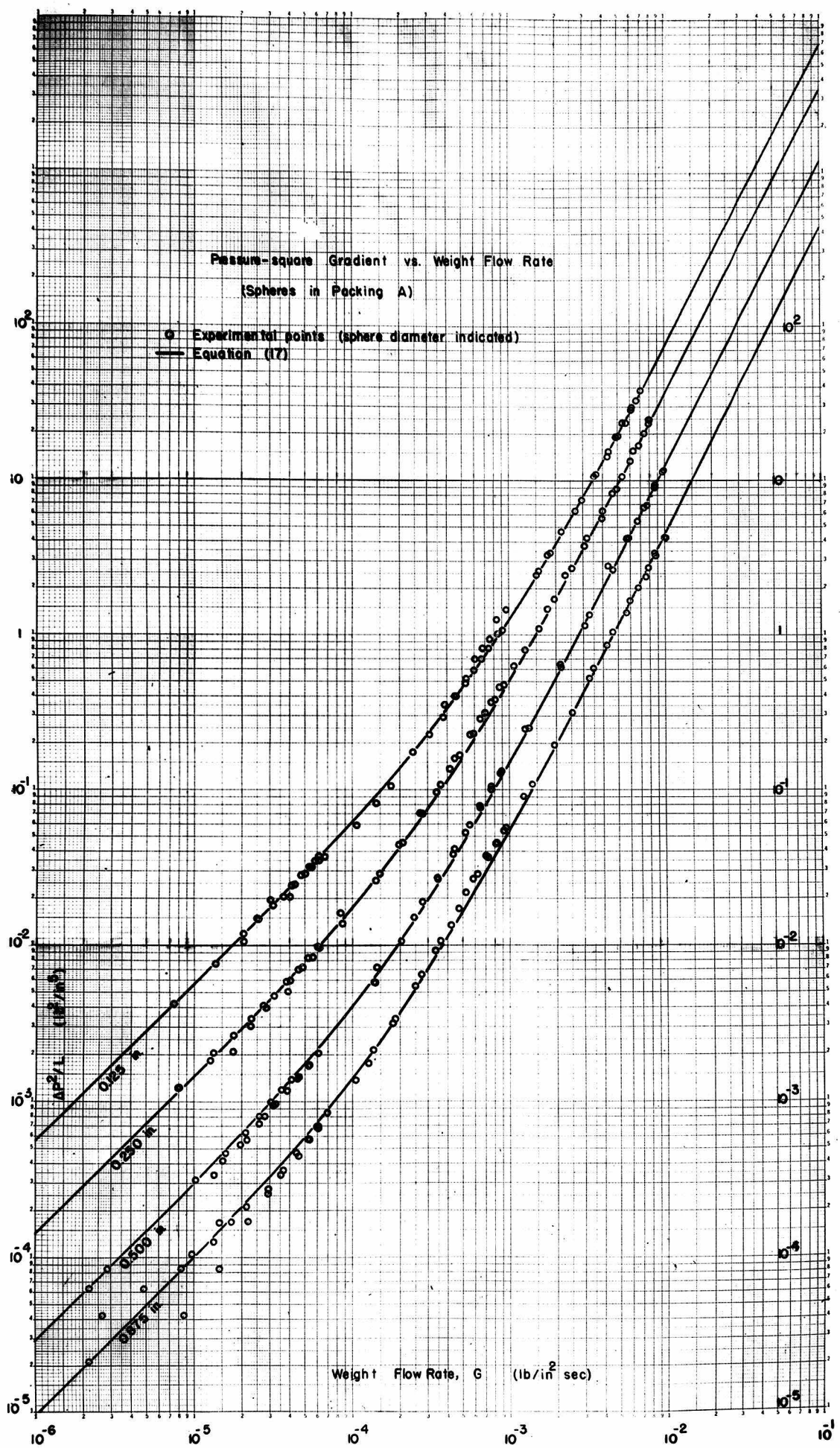
Pressure-square Gradient vs. Weight Flow Rate
(Spheres in Packing A)
Experimental points (sphere diameter indicated)
Equation (17)
0.125 in
0.250 in
0.500 in
0.875 in
ΔP²/L (lb²/in⁵)
Weight Flow Rate, G (lb/in² sec)

Fig. 11

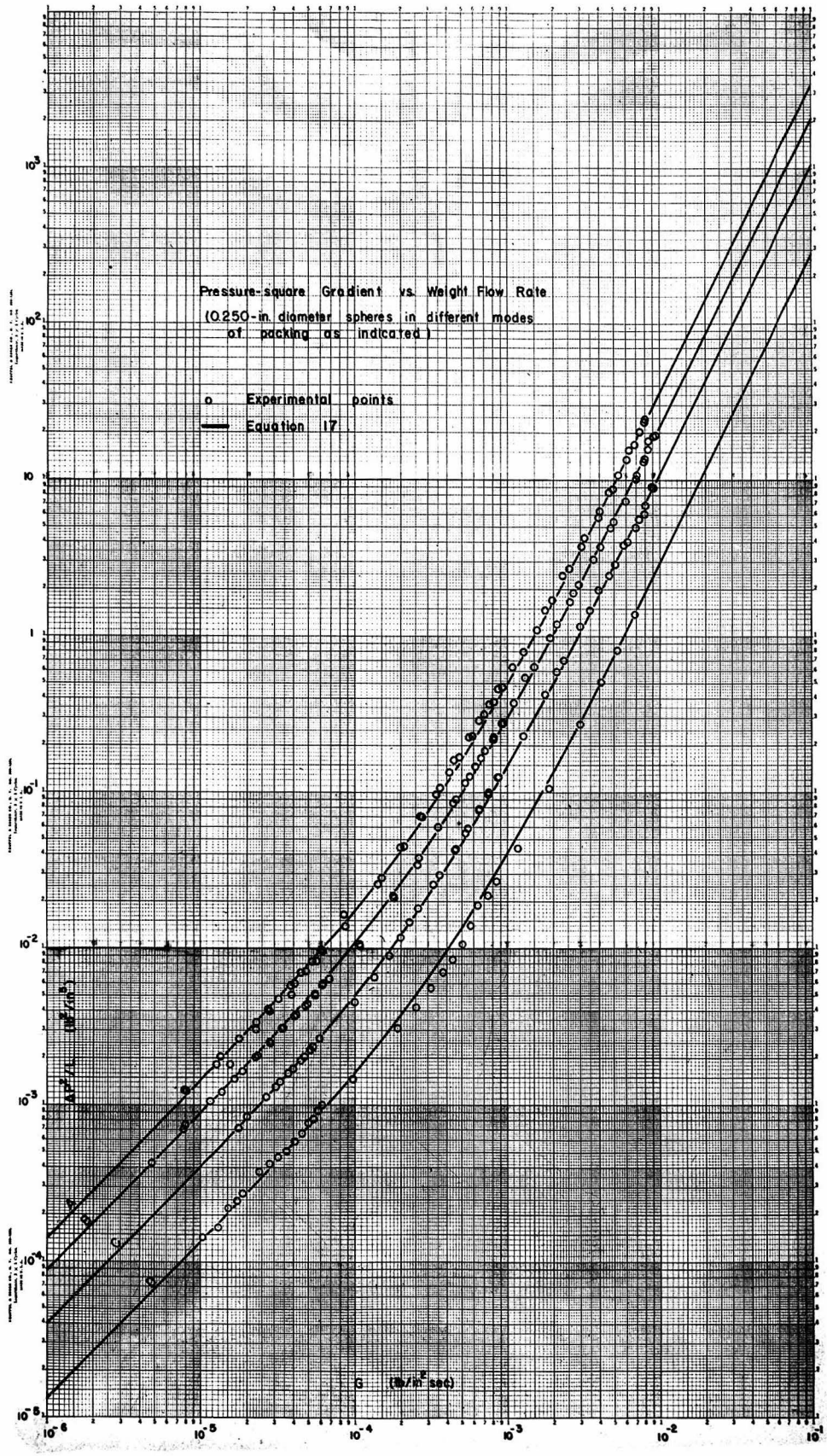
Pressure-square Gradient vs. Weight Flow Rate
(0.250-in. diameter spheres in different modes of packing as indicated)
o Experimental points
Equation 17
A
B
C
D
G (lb/in²sec)

Fig. 12

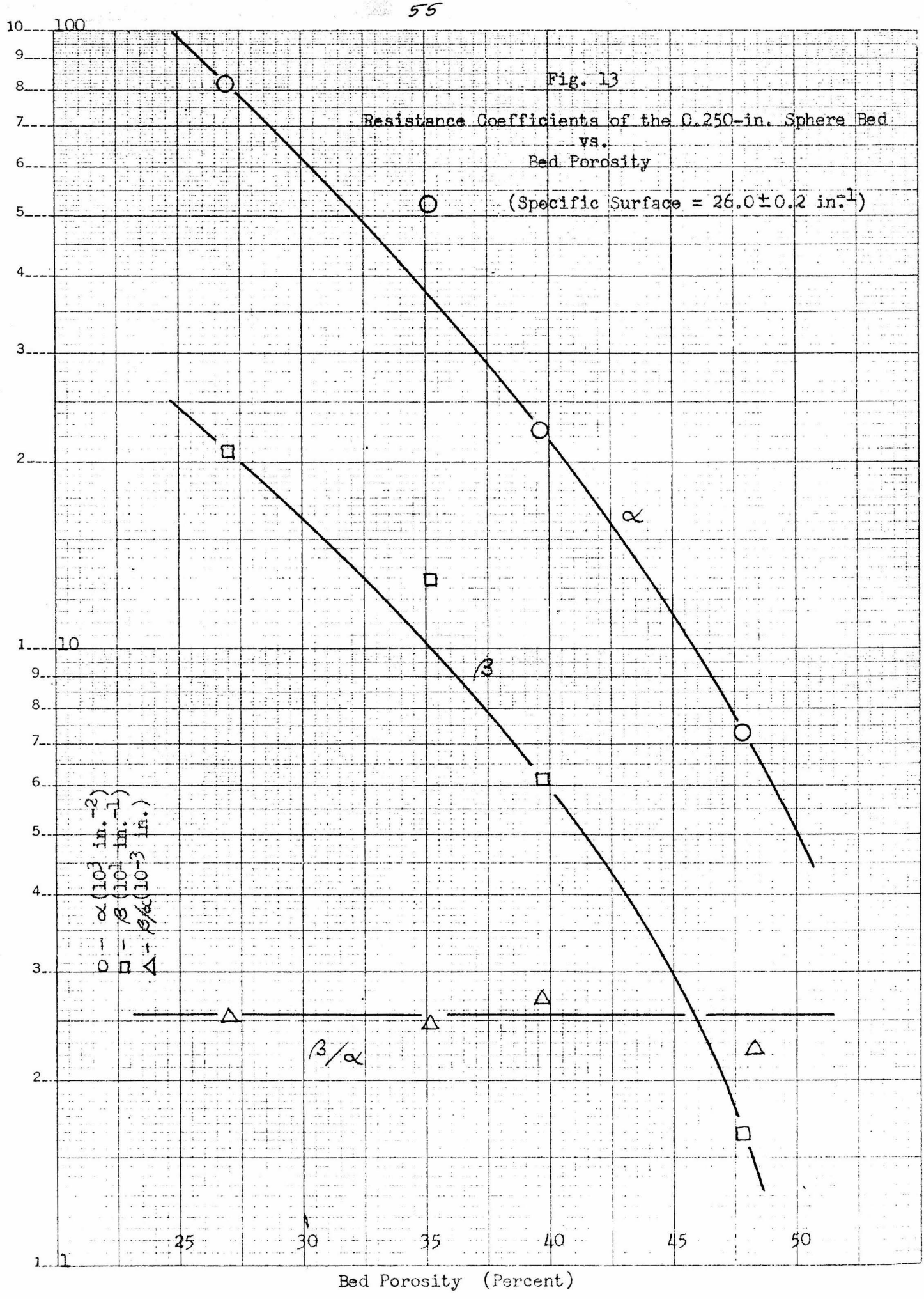
Fig. 13
Resistance Coefficients of the 0.250-in. Sphere Bed
vs.
Bed Porosity
(Specific Surface = 26.0 ± 0.2 in.$^{-1}$)
α
β
β/α
○ - α (10^{3} in.$^{-2}$)
□ - β (10^{1} in.$^{-1}$)
△ - β/α (10^{-3} in.)
100
10
1
25
30
35
40
45
50
Bed Porosity (Percent)

Fig. 14

Comparison of the Viscous Resistance Coefficient as a Function of Porosity with the Predicted Relationships of Kozeny and of Bakhmeteff-Fedoroff

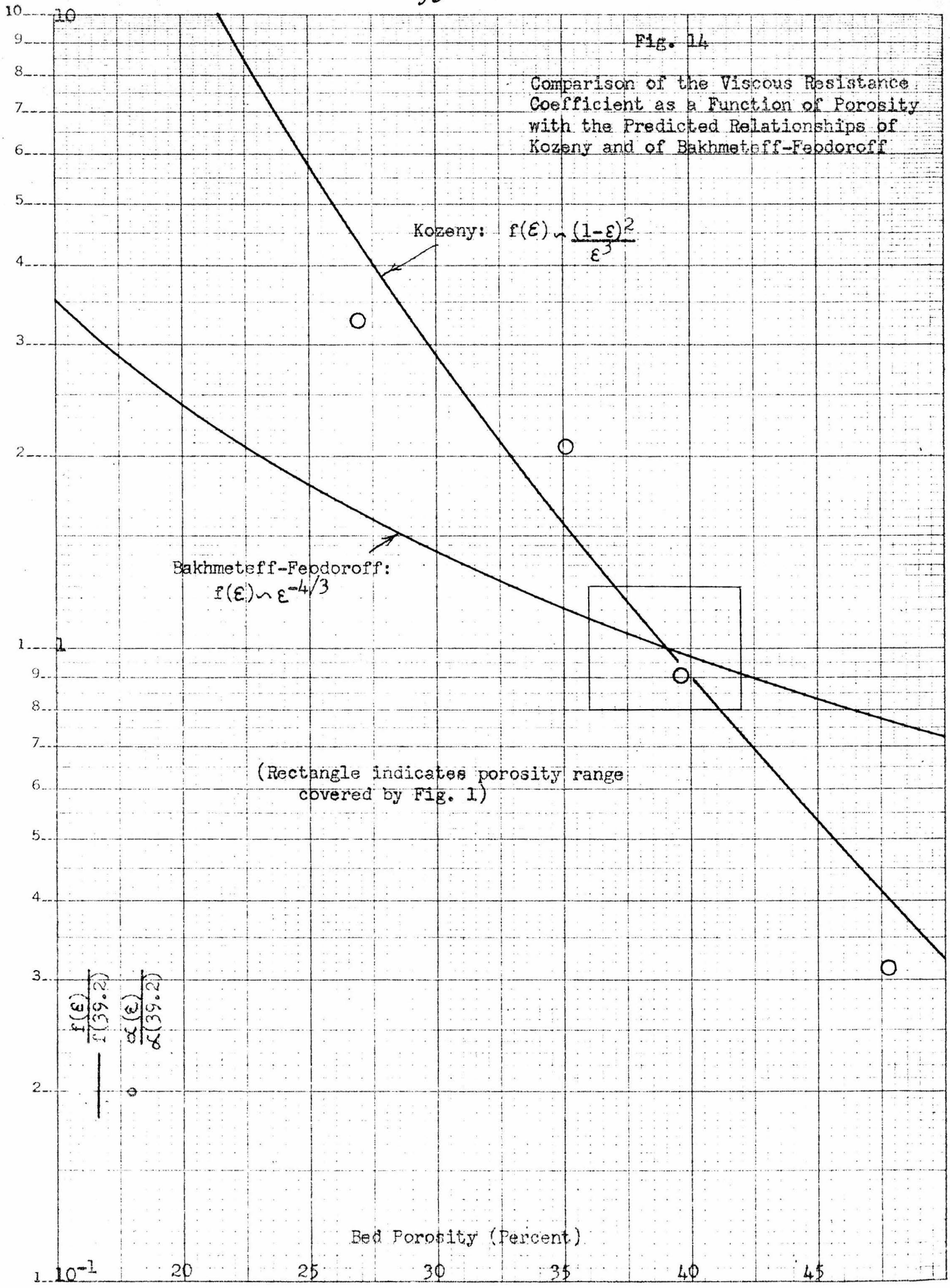

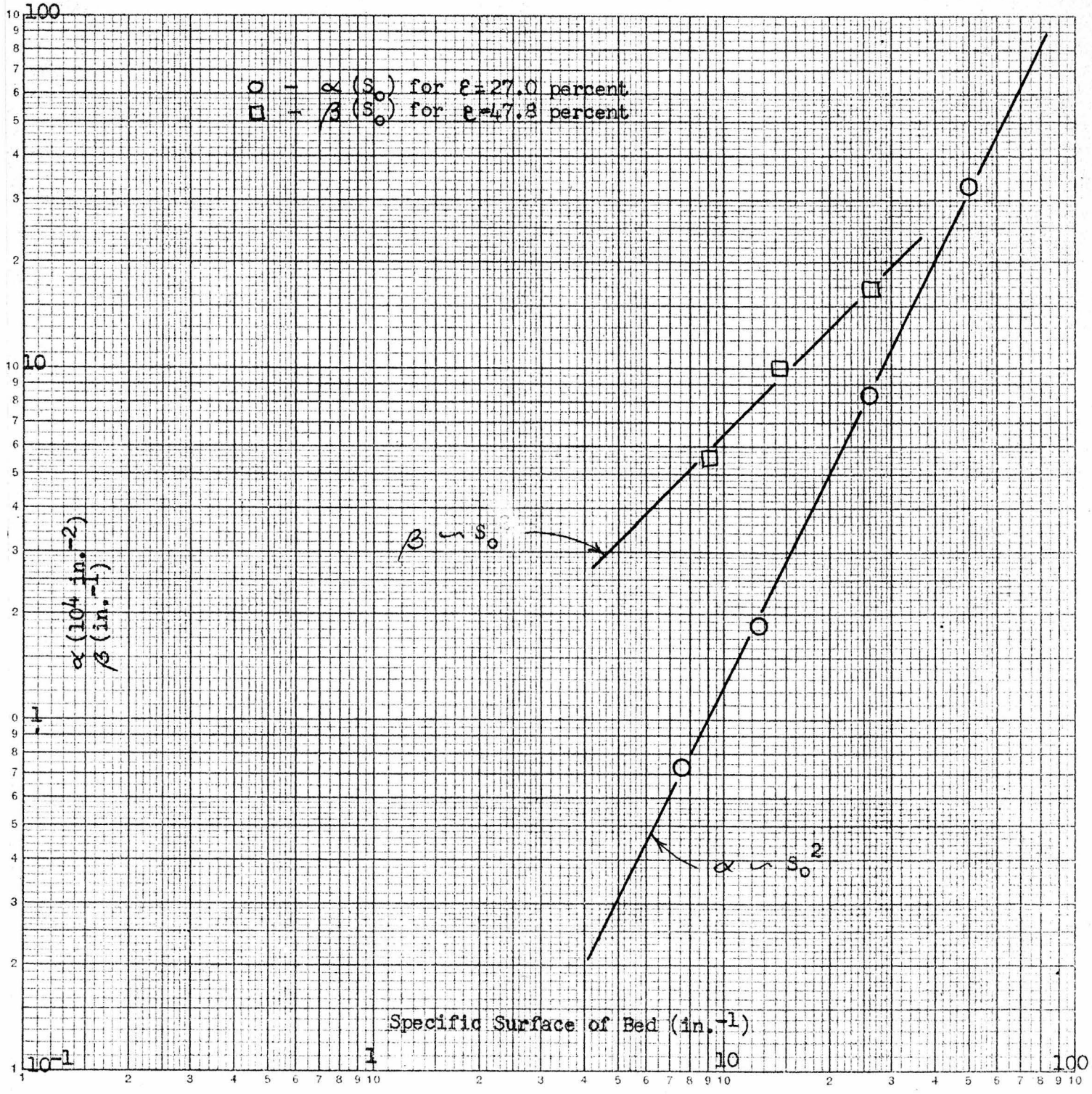

Fig. 15

The Variation of the Viscous and Inertial Resistance with the Specific Surface of the Bed at Constant Porosity

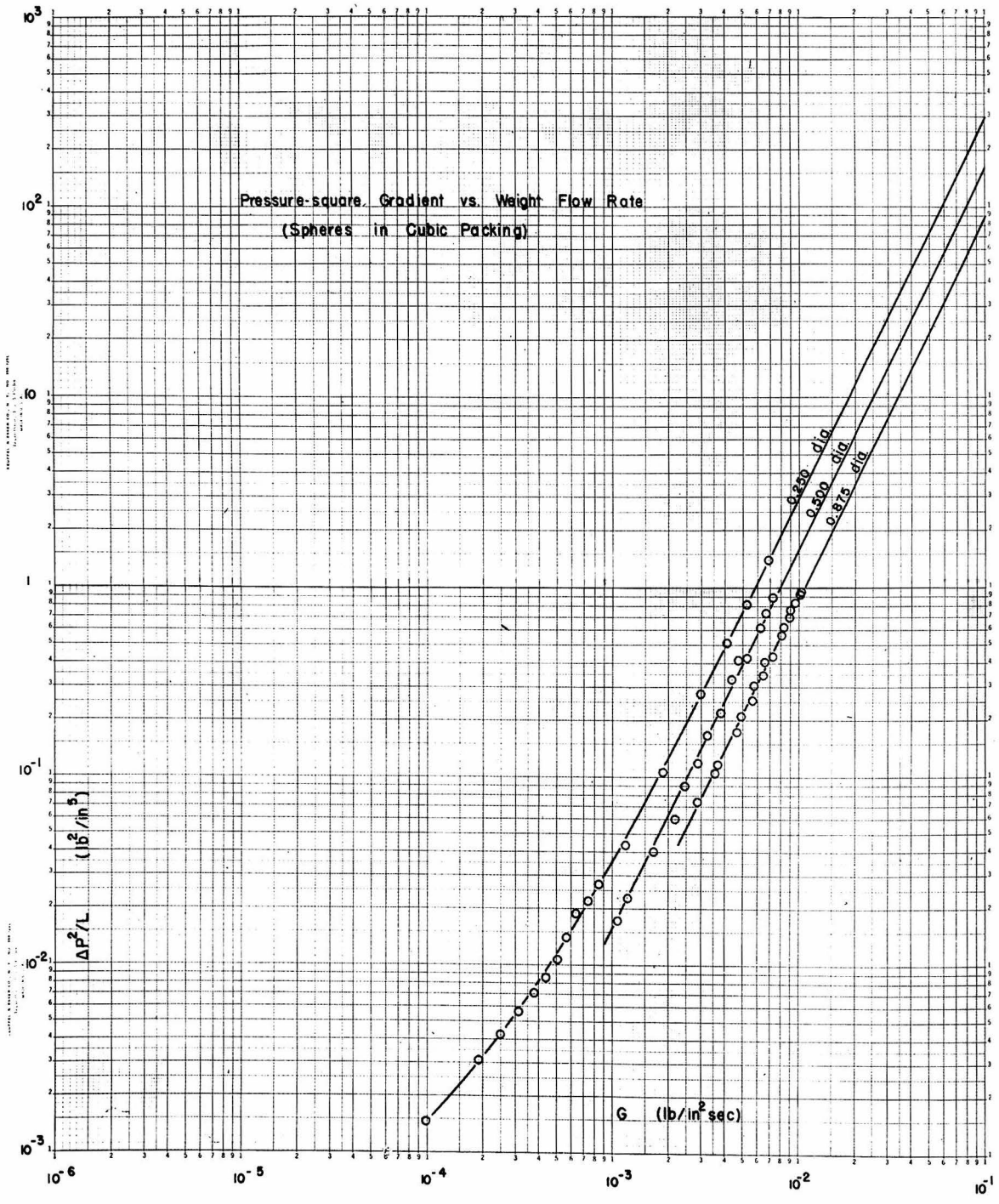
Pressure-square Gradient vs. Weight Flow Rate
(Spheres in Cubic Packing)
0.250 dia.
0.500 dia.
0.875 dia.
ΔP²/L (lb²/in⁵)
G (lb/in² sec)
10³
10²
10
1
10⁻¹
10⁻²
10⁻³
10⁻⁶
10⁻⁵
10⁻⁴
10⁻³
10⁻²
10⁻¹

Fig. 16

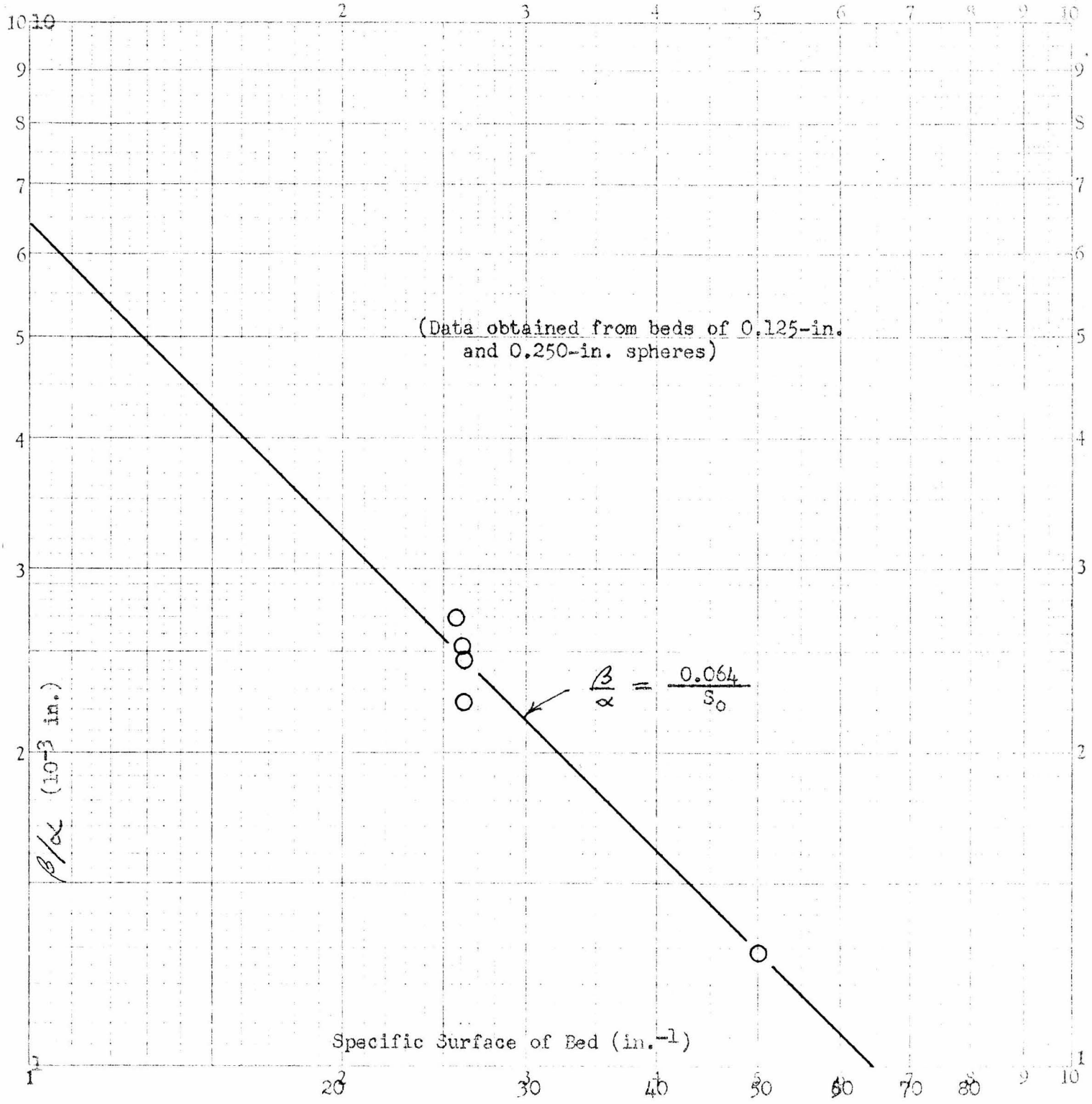

Fig. 17

The Ratio of the Inertial Resistance Coefficient to the Viscous Resistance Coefficient as a Function of the Specific Surface of the Bed.

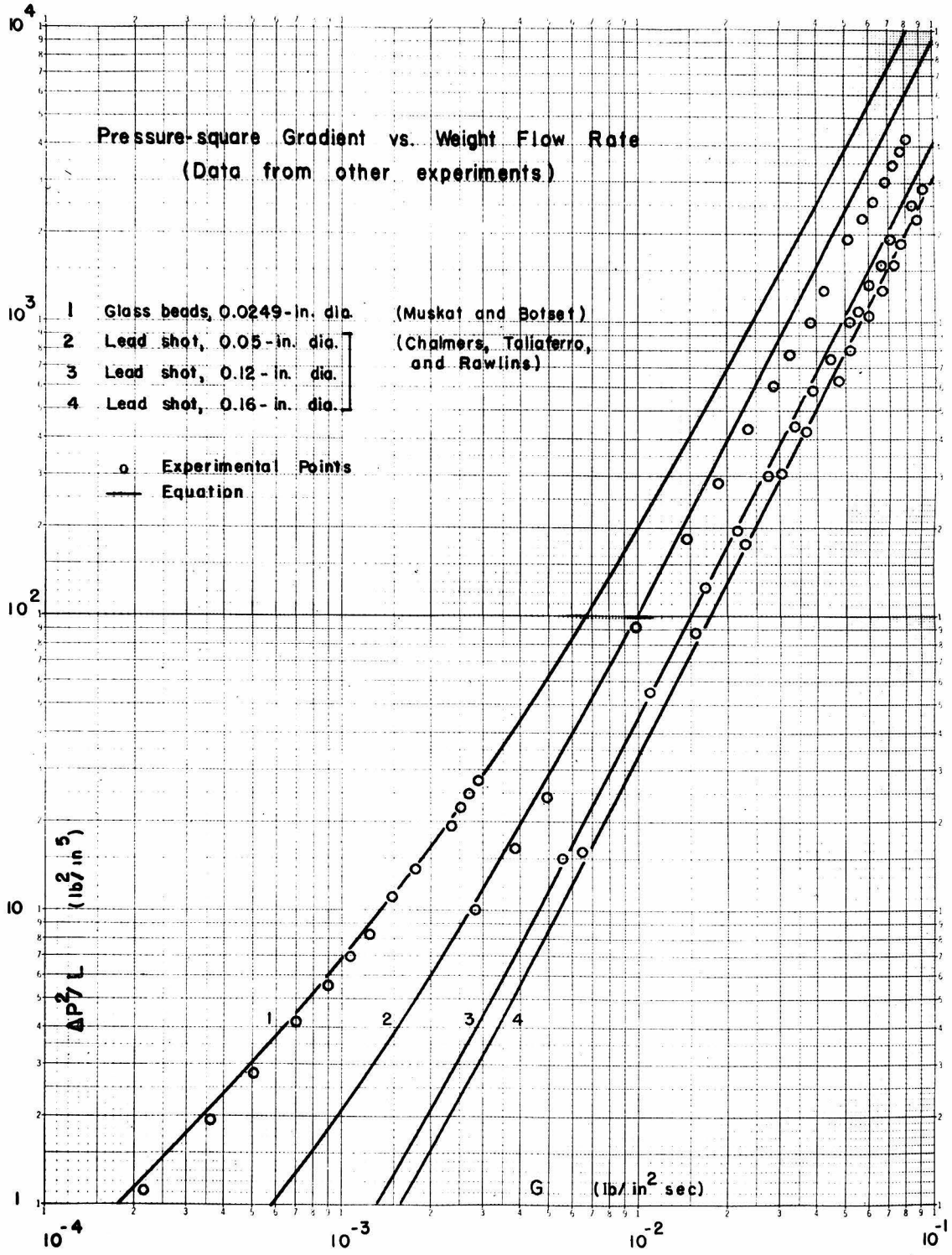
Pressure-square Gradient vs. Weight Flow Rate
(Data from other experiments)
1 Glass beads, 0.0249-in. dia. (Muskat and Botset)
2 Lead shot, 0.05-in. dia.
3 Lead shot, 0.12-in. dia.
4 Lead shot, 0.16-in. dia.
(Chalmers, Taliaferro, and Rawlins)
o Experimental Points
— Equation
$\Delta P^2/L$ (lb²/in⁵)
G (lb/in² sec)
10^4
10^3
10^2
10
1
10^{-4}
10^{-3}
10^{-2}
10^{-1}

Fig. 18

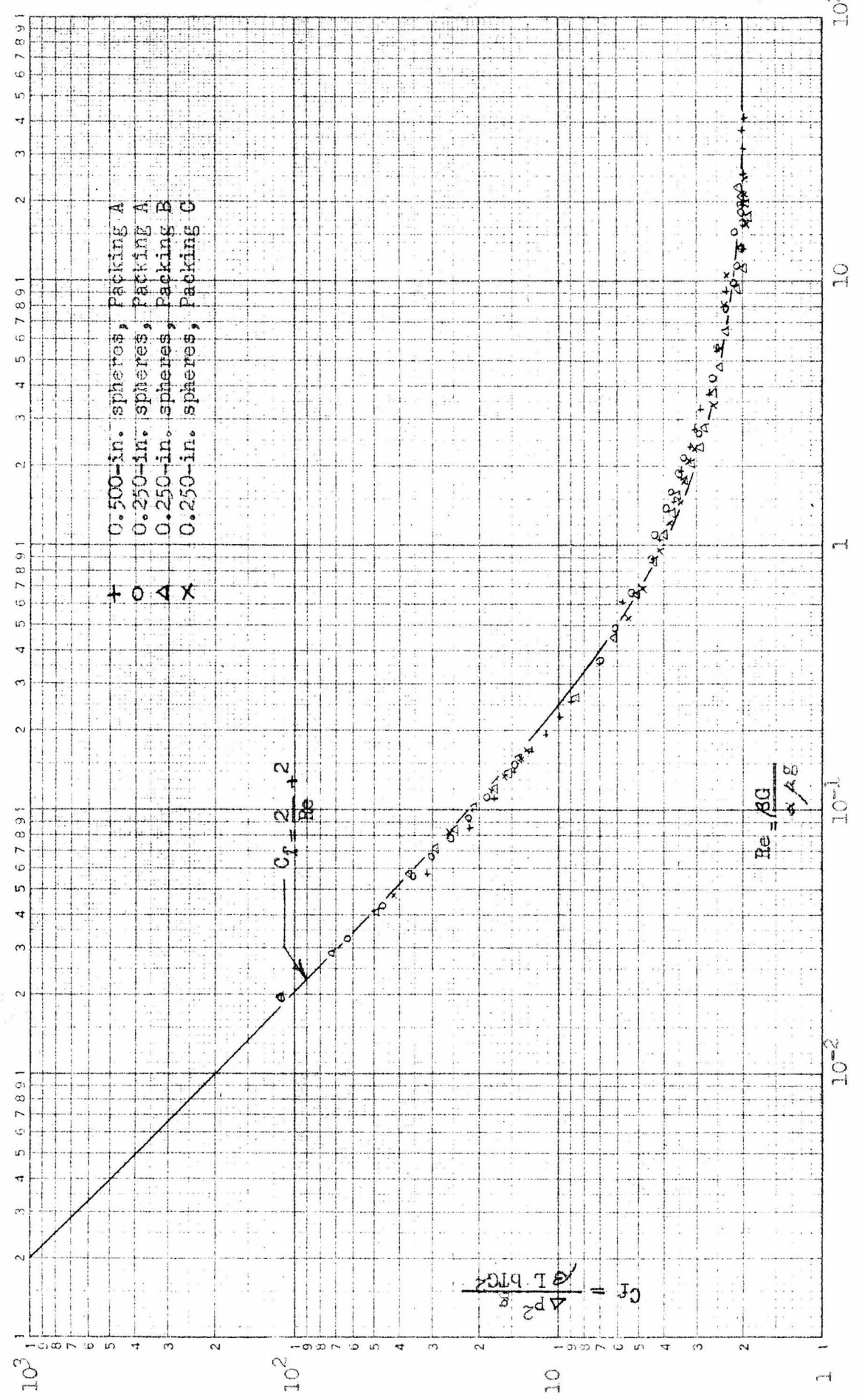

Fig. 19

Friction Factor vs. Reynolds Number Graph of Sphere Bed Data

PART II

NON-STEADY FLOW OF GAS THROUGH A POROUS WALL

I STATEMENT OF THE PROBLEM

A possible application of sweat cooling involves conditions where the pressure difference driving the coolant is subject to sudden changes. The problem requires knowledge of the time needed for the establishment of flow through the porous wall following the sudden application of a pressure gradient across it. If isothermal flow is assumed, the pressure drop equation of the preceding section is valid:

$$\frac{\Delta p^2}{L} = \alpha \left(\frac{2 p_0 \mu}{\sigma_0} \right) G + \beta \left(\frac{2 p_0}{\sigma_0 g} \right) G^2 \tag{1}$$

As an additional simplification, only the viscous flow regime will be considered. Replacing the specific weight σ by the density ρ and the weight flow rate G by the mass flow ρu and introducing the pressure-square gradient, negative in the plus-x direction, we have

$$\rho u = - \frac{1}{\alpha} \left(\frac{p_0}{2 p_0 \mu} \right) \frac{\partial p^2}{\partial x} \tag{2}$$

The equation of continuity for one-dimensional flow through a medium of available porosity ε is

$$\frac{\partial}{\partial x} (\rho u) + \varepsilon \frac{\partial \rho}{\partial t} = 0 \tag{3}$$

Combining Equations (2) and (3) gives

$$- \frac{1}{\alpha} \left(\frac{p_0}{2 p_0 \mu} \right) \frac{\partial^2 p^2}{\partial x^2} + \varepsilon \frac{\partial \rho}{\partial t} = 0 \tag{4}$$

For isothermal flow of a perfect gas,

$$\rho = p\left(\frac{\rho_0}{p_0}\right)$$

or

$$\frac{\partial \rho}{\partial t} = \left(\frac{\rho_0}{p_0}\right)\frac{\partial p}{\partial t}$$

So Equation (4) becomes

$$\frac{\partial^2 p^2}{\partial x^2} = 2\varepsilon\alpha\mu\frac{\partial p}{\partial t}$$

or

$$\frac{\partial}{\partial x}\left(p\frac{\partial p}{\partial x}\right) = \varepsilon\alpha\mu\frac{\partial p}{\partial t} \qquad (5)$$

which is the differential equation governing the pressure distribution throughout the porous medium. The problem of non-steady flow through the porous wall thus involves the solution of Equation (5) subject to the following boundary conditions:

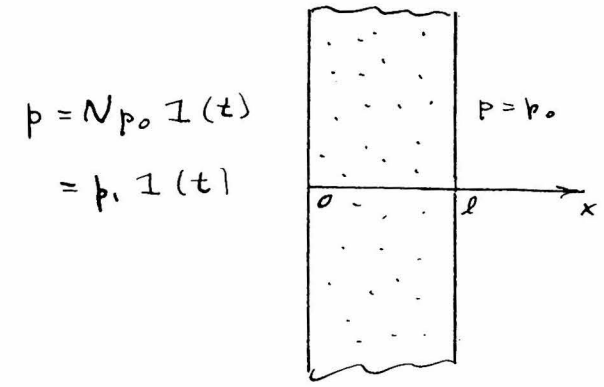

$$p(0, +t) = N p_0 = p_1$$

$$p(\ell, t) = p_0$$

$$p(x, 0) = p_0$$

where p_0 is a reference pressure, N is a number, and ℓ is the wall thickness.

It is convenient to introduce some new dimensionless variables:

$$y = \frac{p}{p_o}$$

$$s = \frac{x}{\ell}$$

$$\tau = \frac{p_o}{\varepsilon \alpha \mu \ell^2} t$$

Since

$$\frac{\partial}{\partial x} = \frac{\partial}{\partial s} \frac{\partial s}{\partial x}$$

Equation (5) becomes

$$\frac{1}{\ell} \frac{\partial}{\partial s} \left(y p_o \frac{p_o}{\ell} \frac{\partial y}{\partial s} \right) = \varepsilon \alpha \mu p_o \frac{\partial y}{\partial t}$$

or

$$\frac{\partial}{\partial s} \left(y \frac{\partial y}{\partial s} \right) = \frac{\varepsilon \alpha \mu \ell^2}{p_o} \frac{\partial y}{\partial t}$$

And since

$$\frac{\partial}{\partial t} = \frac{\partial}{\partial \tau} \frac{\partial \tau}{\partial t}$$

the boundary value problem thus becomes

$$\frac{\partial}{\partial s} \left(y \frac{\partial y}{\partial s} \right) = \frac{\partial y}{\partial \tau} \qquad (6)$$

where

$$y(0, +\tau) = N$$

$$y(1, \tau) = 1$$

$$y(.5, 0) = 1$$

This non linear parabolic equation is not solvable by standard

analytical methods, but numerical solutions are obtainable if the differential equation is approximated by a finite difference equation. In this case, a convenient means of solution was afforded by satisfying the difference equation with an electrical analogy suggested by Professor C. H. Wilts.

II THE ELECTRICAL ANALOGY

A difference equation equivalent to Equation (6) can be written (see Figure 1) as

$$\left\{ \frac{y_{n+\frac{1}{2},m}\left[\frac{y_{n+1,m}-y_{n,m}}{\Delta s_{n+\frac{1}{2}}}\right] - y_{n-\frac{1}{2},m}\left[\frac{y_{n,m}-y_{n-1,m}}{\Delta s_{n-\frac{1}{2}}}\right]}{\Delta s_n} \right\}$$

$$= \frac{1}{2}\left\{ \frac{y_{n,m+1}-y_{n,m}}{\Delta \tau_{m+\frac{1}{2}}} + \frac{y_{n,m}-y_{n,m-1}}{\Delta \tau_{m-\frac{1}{2}}} \right\} \qquad (7)$$

Multiplying both sides by Δs_n one gets

$$\frac{y_{n+\frac{1}{2},m}}{\Delta s_{n+\frac{1}{2}}}\left[y_{n+1,m}-y_{n,m}\right] - \frac{y_{n-\frac{1}{2},m}}{\Delta s_{n-\frac{1}{2}}}\left[y_{n,m}-y_{n-1,m}\right]$$

$$-\frac{\Delta s_n}{2\Delta \tau_{m+\frac{1}{2}}}\left[y_{n,m+1}-y_{n,m}\right] - \frac{\Delta s_n}{2\Delta \tau_{m-\frac{1}{2}}}\left[y_{n,m}-y_{n,m-1}\right] = 0 \qquad (8)$$

Now consider the network shown in Figure 2. Kirchoff's Law requires that the sum of the currents entering the central junction be zero:

$$\Sigma I = \frac{\varphi_{n+1,m} - \varphi_{n,m}}{Z_{n+\frac{1}{2},m}} + \frac{\varphi_{n-1,m} - \varphi_{n,m}}{Z_{n-\frac{1}{2},m}} + \frac{\varphi_{n,m+1} - \varphi_{n,m}}{Z_{n,m+\frac{1}{2}}} + \frac{\varphi_{n,m-1} - \varphi_{n,m}}{Z_{n,m-\frac{1}{2}}} \qquad (9)$$

$$= 0$$

Thus, if we set

$$Z_{n+\frac{1}{2},m} = a\,\frac{\Delta S_{n+\frac{1}{2}}}{y_{n+\frac{1}{2},m}} \qquad Z_{n,m+\frac{1}{2}} = -\frac{a\,2\Delta\tau_{m+\frac{1}{2}}}{\Delta S_n}$$

$$Z_{n-\frac{1}{2},m} = a\,\frac{\Delta S_{n-\frac{1}{2}}}{y_{n-\frac{1}{2},m}} \qquad Z_{n,m-\frac{1}{2}} = \frac{a\,2\Delta\tau_{m-\frac{1}{2}}}{\Delta S_n} \qquad (10)$$

(where a is an arbitrary constant) and applying boundary voltages equal numerically to the boundary values of the pressure ratio y, then the voltage at any point n,m is equal to the value of y at

$$S = \sum_{i=1}^{n} \Delta S_{i-\frac{1}{2}}$$

$$\tau = \sum_{i=1}^{m} \Delta \tau_{i-\frac{1}{2}}$$

From Equation (10) it can be seen that in order to satisfy Equation (8) three of the four impedance elements joining each node of the electrical network must be opposite in sign to the fourth. This requirement was met by the use of an alternating boundary potential together with a network of inductances and capacitances, as shown in Figure 3. The vertical impedances are shown by Equation (10) to be constant, depending only upon the selected intervals of

space and time. The non-linear nature of the problem, however, is manifested in the horizontal impedances, which are seen to be functions of the pressure ratio obtaining at each point in question. This dependence required an iterative process of solution, in which the initial values of the horizontal impedances were determined from a rough estimate of y as a function of s for various values of τ .

III THE PROCEDURE OF SOLUTION

Three typical boundary value problems of the type described above were solved with the use of the Electric Analog Computer by Professor Wilts and the writer. Problems with increasing degrees of non-linearity were studied by considering cases where N (the ratio of the applied boundary pressure to the initial pressure) assumed the values of 2, 4, and 10.

From Figure 3 it may be seen that the time variable could not approach infinity in the static analog, since only a finite number of time increments were available. This made it necessary to choose the size of the time interval such that steady state conditions were reached or closely approximated after eight time increments for the abrupt termination of the network in the time direction after steady state has been reached has a negligible effect upon the solution for smaller values of time. It was found by experimentation that a value of the dimensionless increment $\Delta\tau$ of about 0.010 was large enough to give approximately steady state conditions in the case of

the lowest boundary pressure ratio. This interval was halved in the case of N = 10.

The convergence of the iteration process described above was found to be surprisingly rapid. For the case of N = 2, the measured potentials corresponding to the dimensionless pressure y were found to have approached to within one percent of their final value after only one iteration. For the more non-linear cases (N = 4, 10), a larger number of iterations was required for convergence. The rapidity of the process, of course, depends upon the accuracy of the initial estimate of the pressure distribution.

IV RESULTS AND CONCLUSIONS

The final values of y which were obtained in each of the three cases described above are summarized in Table I. When these data were plotted to give pressure distribution curves, it was discovered that steady state conditions had not always been approached closely enough to eliminate completely the influence of the network termination in the time direction upon the solutions for the largest measured values of time. It was felt that a repetition of the solution would not be necessary, that the slight scatter of the points with time resulting from the abrupt termination could be removed equally well by smoothing the curve. For this purpose, the values of y given Table I were plotted versus τ for various values of s, as shown in Figures 4, 5, and 6. The pressure distri-

butions for each of the three cases were computed from the smooth curves of these figures and are presented in Figures 7, 8, and 9. It is interesting to observe the change in the shape of the curves as the boundary pressure ratio is increased.

As was initially stated, the primary interest in the problem was in flow through the low pressure face of the porous wall. According to Equation (2) the flow rate is proportional to the pressure-square gradient. In order to determine this gradient the data of Figures 4, 5, and 6 were used to calculate the curves of y^2 versus s presented in Figures 10, 11, and 12. The values of $\partial y^2/\partial s$ at $s = 1$, graphically determined from these curves, are plotted versus τ in Figure 13. The fact that steady state conditions were not realized required an extrapolation of the curves of Figure 13 to the values of the steady state slope. This extrapolation makes the results only semi-quantitative, but the trend is evident. As was expected, the time interval τ_s required for the establishment of steady flow through a porous wall following the sudden application of a pressure to one side of the wall is seen to decrease as the ratio of the applied pressure to the initial pressure is increased. Since a five-fold increase in the pressure ratio effected only about a 40 percent decrease in τ_s, however, it may be concluded that the critical time interval is not greatly influenced by the ratio of the boundary pressures. It may also be seen that the time required for the appearance of any flow at all is also only slightly sensitive to the pressure ratio.

NOMENCLATURE

a	A constant
d	Derivative notation
g	Acceleration due to gravity $[LT^{-2}]$
I	Electric Current
i	A subscript
L	A length variable $[L]$
l	Thickness of wall $[L]$
m	A subscript
N	A number
n	A subscript
P	Pressure $[ML^{-1}T^{-2}]$
Q	Quantity of electricity $[Q]$
S	A dimensionless length variable
t	Time $[T]$
u	Fluid velocity $[LT^{-1}]$
x	A length variable $[L]$
y	A dimensionless pressure
Z	Electrical impedence $[MQ^{-2}L^{2}T^{-1}]$
α	Viscous resistance coefficient $[L^{-2}]$
β	Inertial resistance coefficient $[L^{-1}]$
ε	Porosity (dimensionless)
μ	Dynamic viscosity $[ML^{-1}T^{-1}]$
ρ	Fluid density $[ML^{-3}]$
σ	Specific weight $[ML^{-2}T^{-2}]$
τ	Dimensionless time
φ	Electrical potential $[MQ^{-1}L^{2}T^{-2}]$

TABLE I

Non-Steady Pressure Distribution in a Porous Wall for Three Different Ratios of Applied Pressure to Initial Pressure, Calculated by Electrical Analogy

Dimensionless Time,	Dimensionless Distance, S								
	0	1/8	1/4	3/8	1/2	5/8	3/4	7/8	1
				Case 1: N = 2					
0	2.000	1.000	1.000	1.000	1.000	1.000	1.000	1.000	1.000
.0169	2.000	1.682	1.483	1.245	1.118	1.048	1.015	1.002	1.000
.0322	2.000	1.798	1.617	1.438	1.287	1.166	1.087	1.036	1.000
.0491	2.000	1.842	1.685	1.536	1.392	1.266	1.161	1.074	1.000
.0644	2.000	1.864	1.726	1.592	1.463	1.333	1.220	1.112	1.000
.0813	2.000	1.878	1.754	1.631	1.501	1.377	1.252	1.130	1.000
.0966	2.000	1.884	1.767	1.654	1.532	1.407	1.282	1.147	1.000
.1135	2.000	1.888	1.775	1.663	1.546	1.423	1.293	1.153	1.000
.1288	2.000	1.900	1.792	1.680	1.564	1.438	1.307	1.163	1.000
				Case 2: N = 4					
0	4.00	1.00	1.00	1.00	1.00	1.00	1.00	1.00	1.00
.0169	4.00	3.07	2.30	1.68	1.26	1.04	1.00	1.00	1.00
.0322	4.00	3.43	2.83	2.27	1.76	1.36	1.12	1.03	1.00
.0491	4.00	3.55	3.08	2.59	2.13	1.70	1.36	1.14	1.00
.0644	4.00	3.61	3.22	2.79	2.37	1.98	1.61	1.29	1.00
.0813	4.00	3.67	3.31	2.92	2.53	2.17	1.79	1.41	1.00
.0966	4.00	3.70	3.37	3.02	2.67	2.31	1.92	1.50	1.00
.1135	4.00	3.72	3.41	3.08	2.73	2.38	2.00	1.56	1.00
.1288	4.00	3.73	3.43	3.14	2.81	2.46	2.06	1.61	1.00
				Case 3: N = 10					
0	10.0	1.00	1.00	1.00	1.00	1.00	1.00	1.00	1.00
.00645	10.0	7.60	5.46	3.78	2.17	1.13	1.00	1.00	1.00
.0169	10.0	8.59	7.06	5.53	3.98	2.53	1.43	1.00	1.00
.0254	10.0	8.91	7.73	6.46	5.13	3.83	2.57	1.56	1.00
.0338	10.0	9.06	8.03	6.99	5.86	4.69	3.50	2.33	1.00
.0423	10.0	9.17	8.20	7.35	6.35	5.24	4.15	2.83	1.00
.0507	10.0	9.21	8.41	7.55	6.62	5.58	4.47	3.12	1.00
.0591	10.0	9.26	8.52	7.66	6.77	5.79	4.66	3.28	1.00
.0688	10.0	9.30	8.57	7.79	6.93	5.92	4.82	3.40	1.00

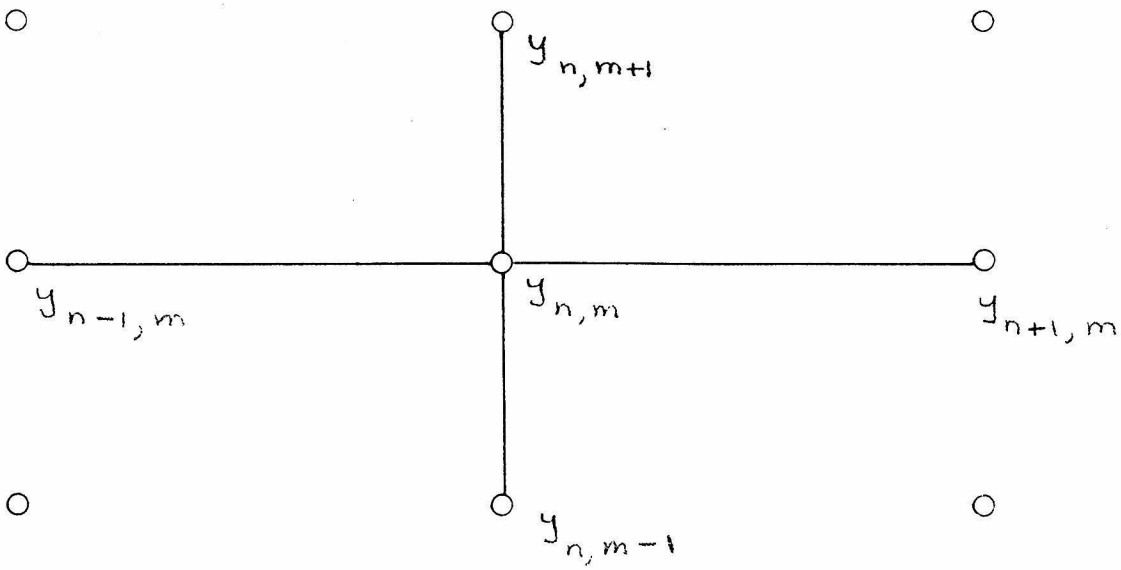

Fig. 1

Typical Mesh Element for Difference Equation

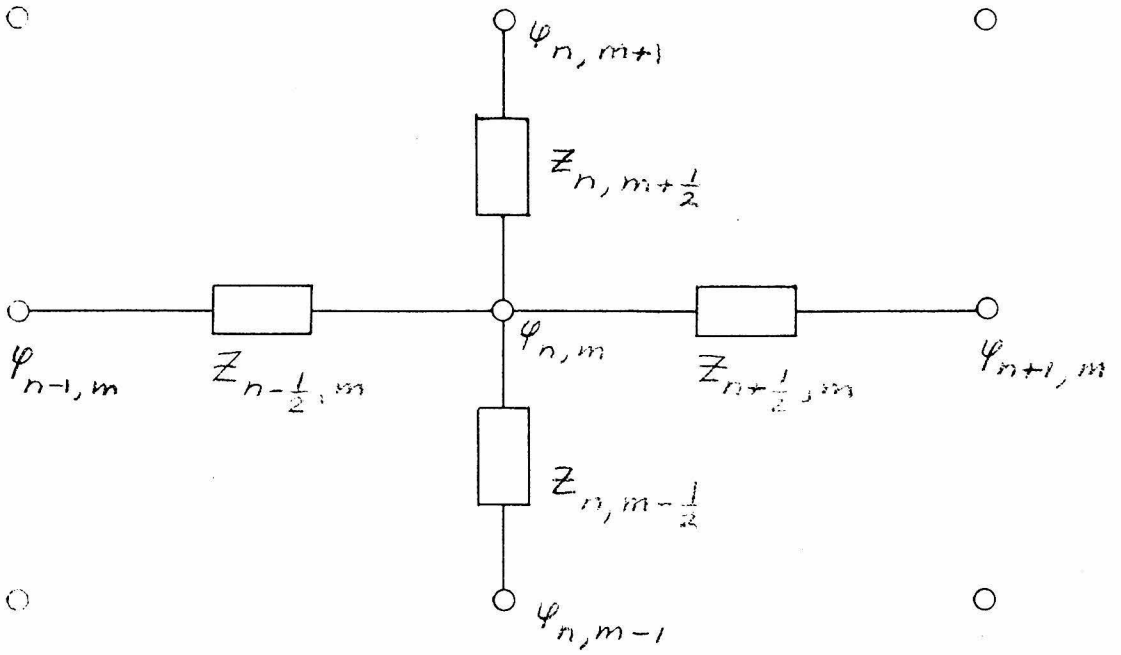

Fig. 2

Typical Node of an Electrical Network

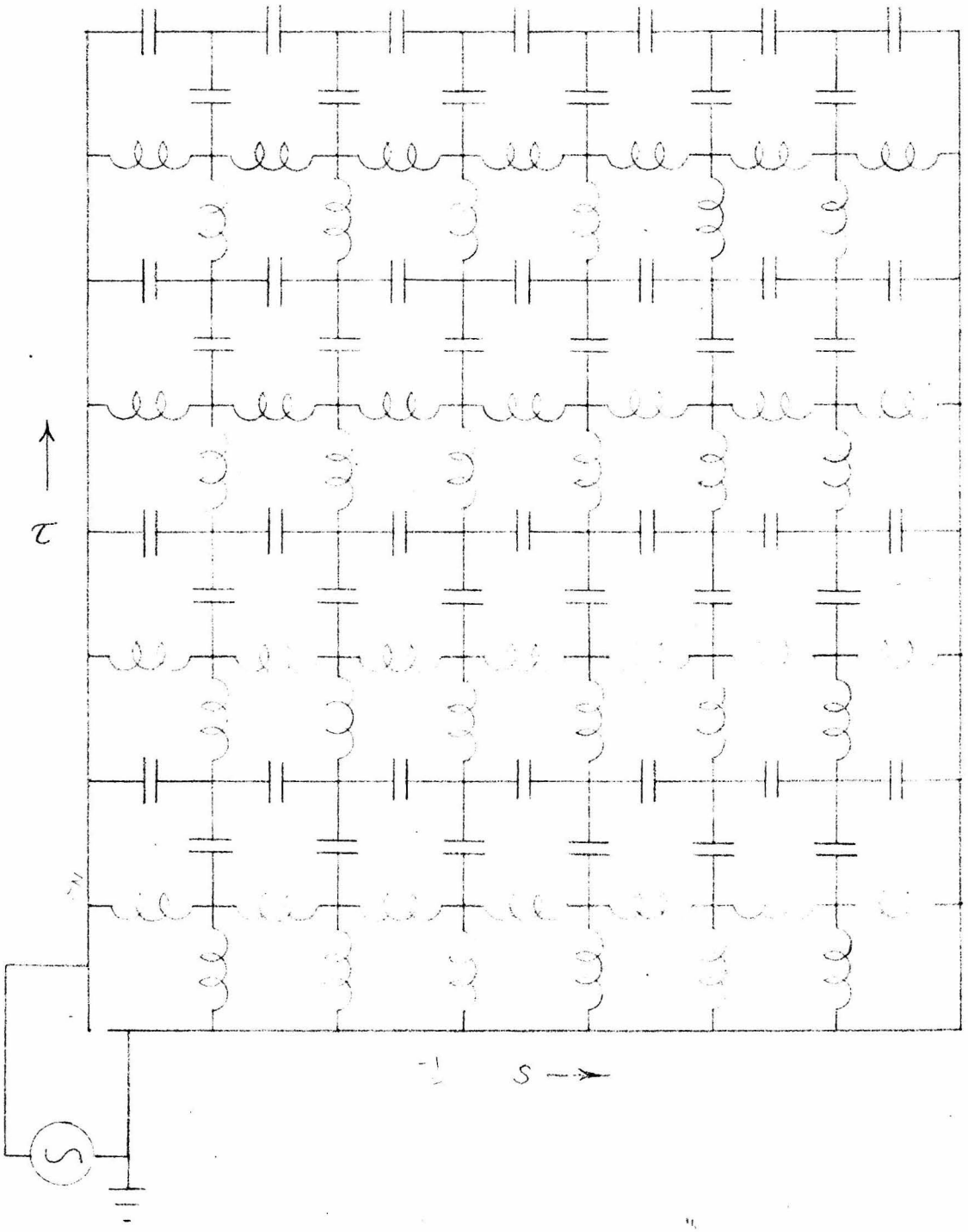

Fig. 3

Analogous Electrical Network Satisfying the Given Difference Equation

Fig. 4

Dimensionless Pressure vs. Dimensionless Time at Various Positions

Case 1: N = 2

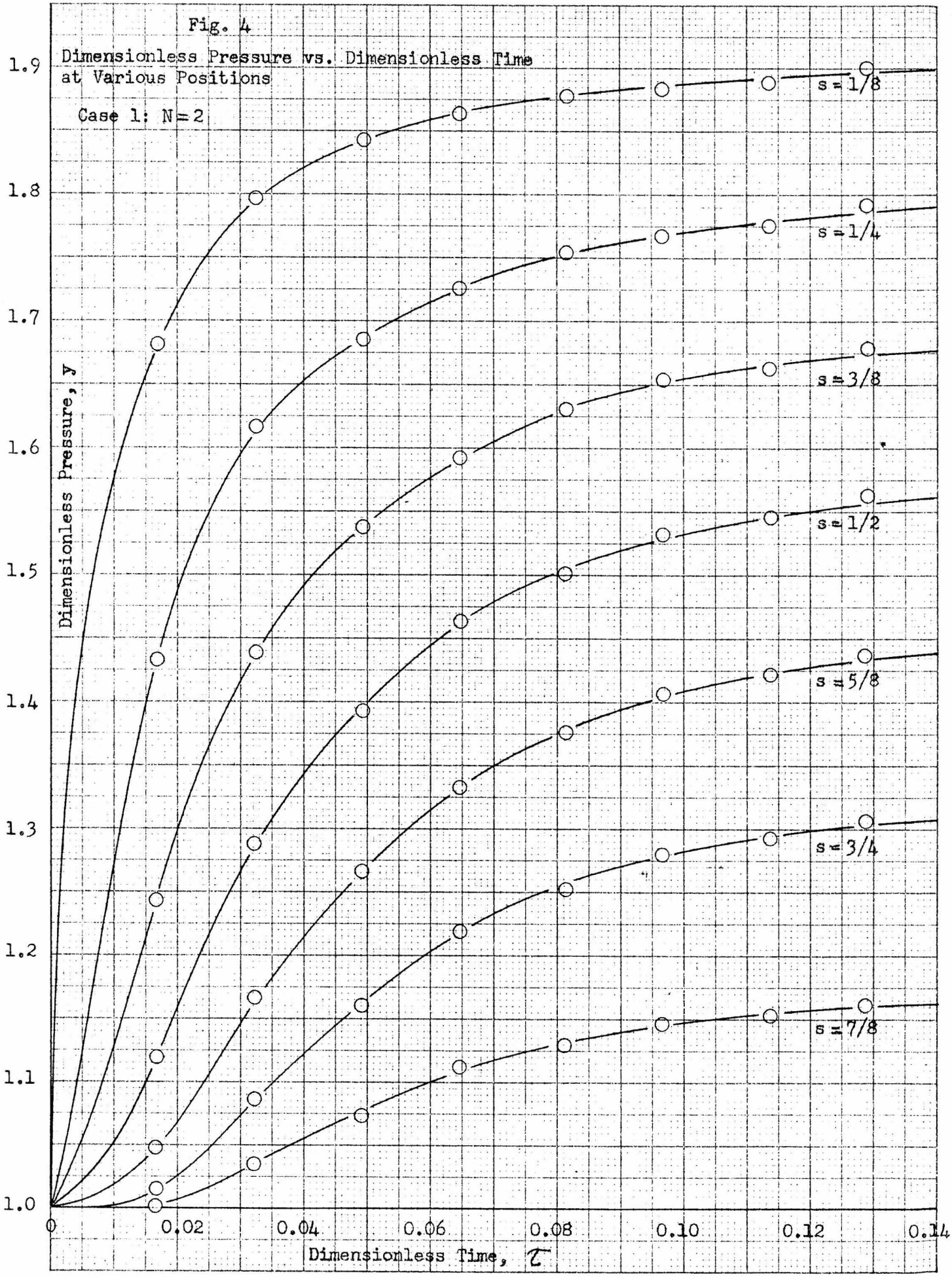

Fig. 5
Dimensionless Pressure vs. Dimensionless Time
at Various Positions

Case 2: N=4

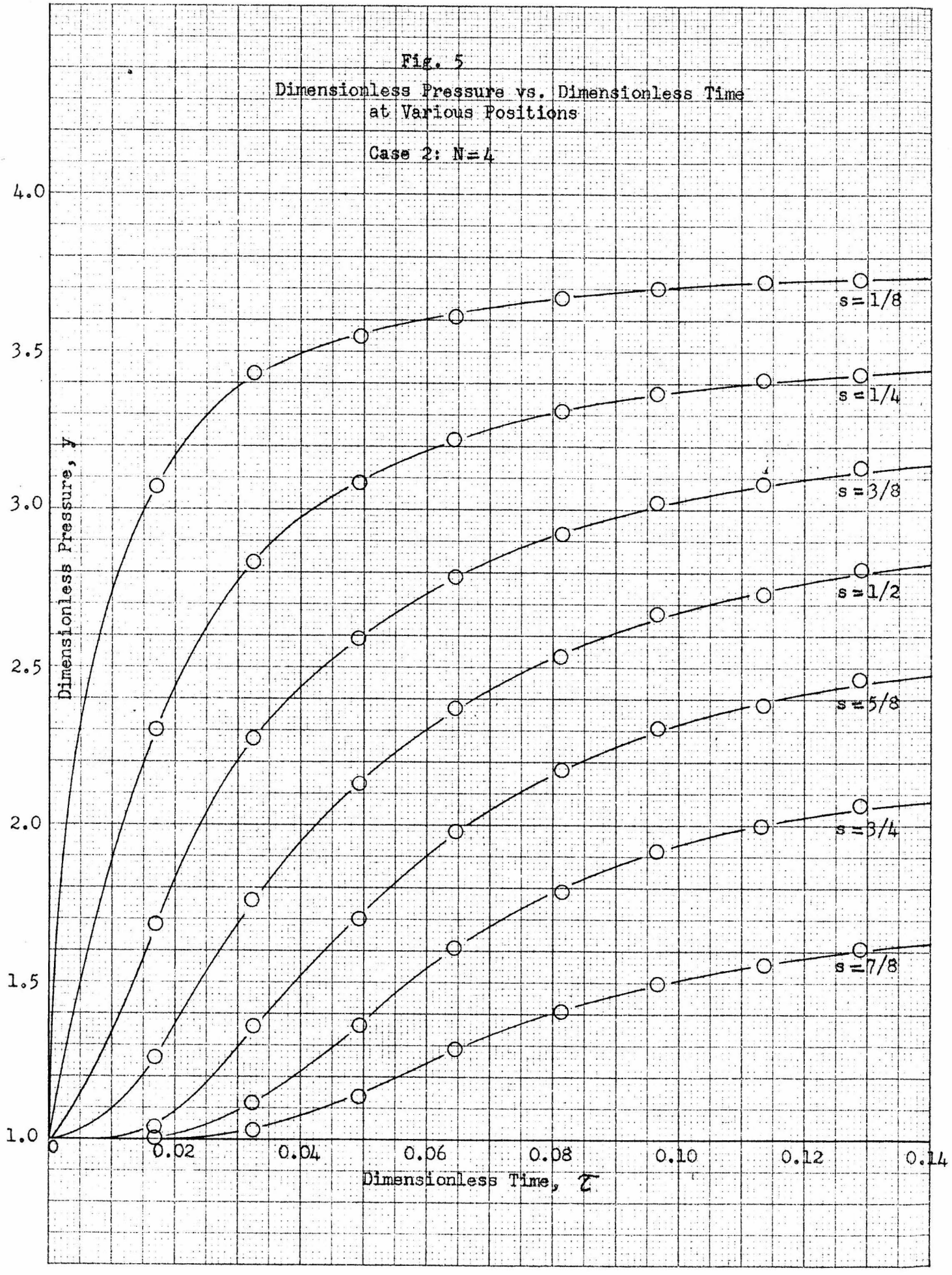

Fig. 6

Dimensionless Pressure vs. Dimensionless Time at Various Positions

Case 3: N = 10

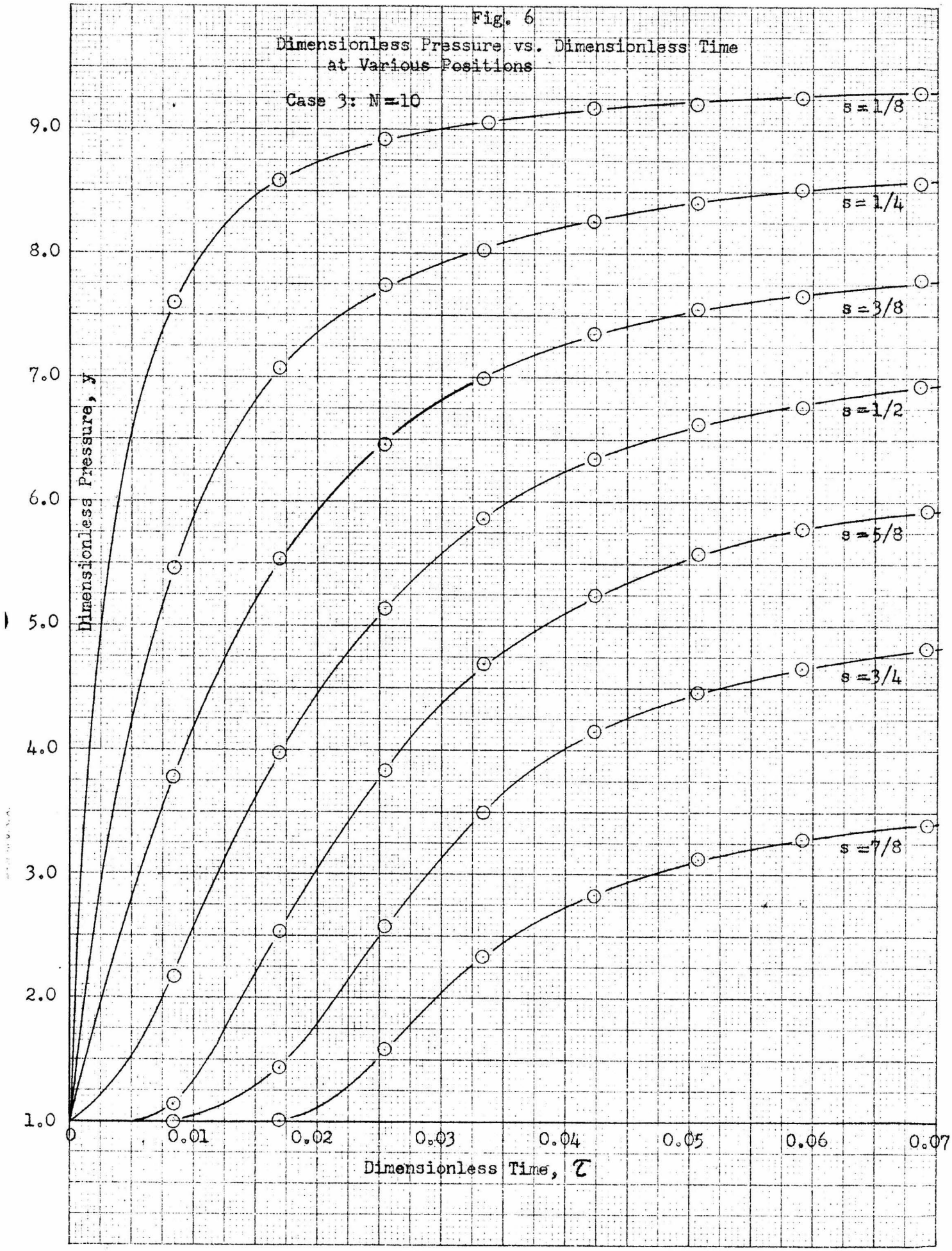

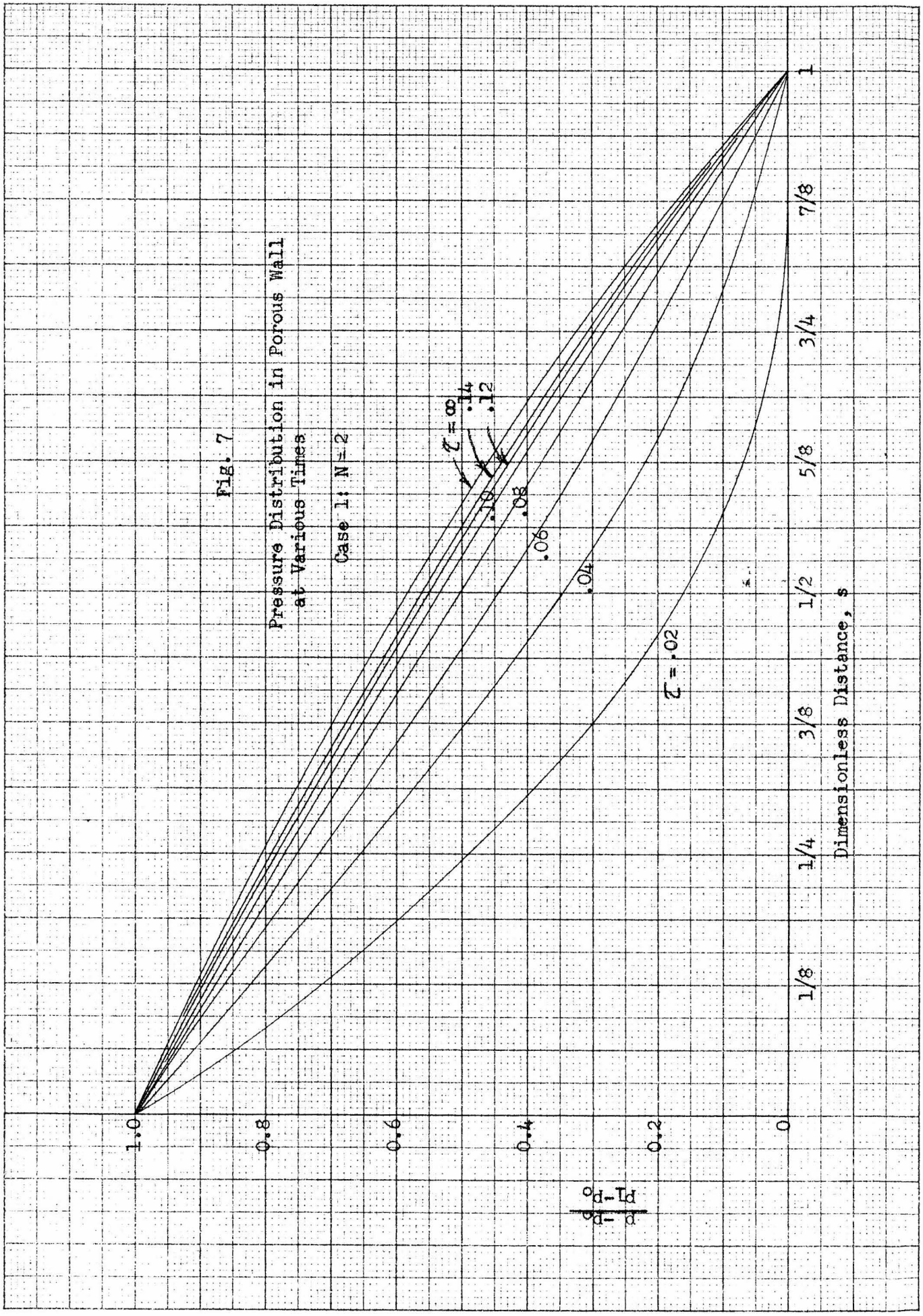
Fig. 7
Pressure Distribution in Porous Wall
at Various Times
Case 1: N=2
$\tau = \infty$
.14
.12
.10
.08
.06
.04
$\tau = .02$
$\frac{p - p_o}{p_1 - p_o}$
1.0
0.8
0.6
0.4
0.2
0
1/8
1/4
3/8
1/2
5/8
3/4
7/8
1
Dimensionless Distance, s

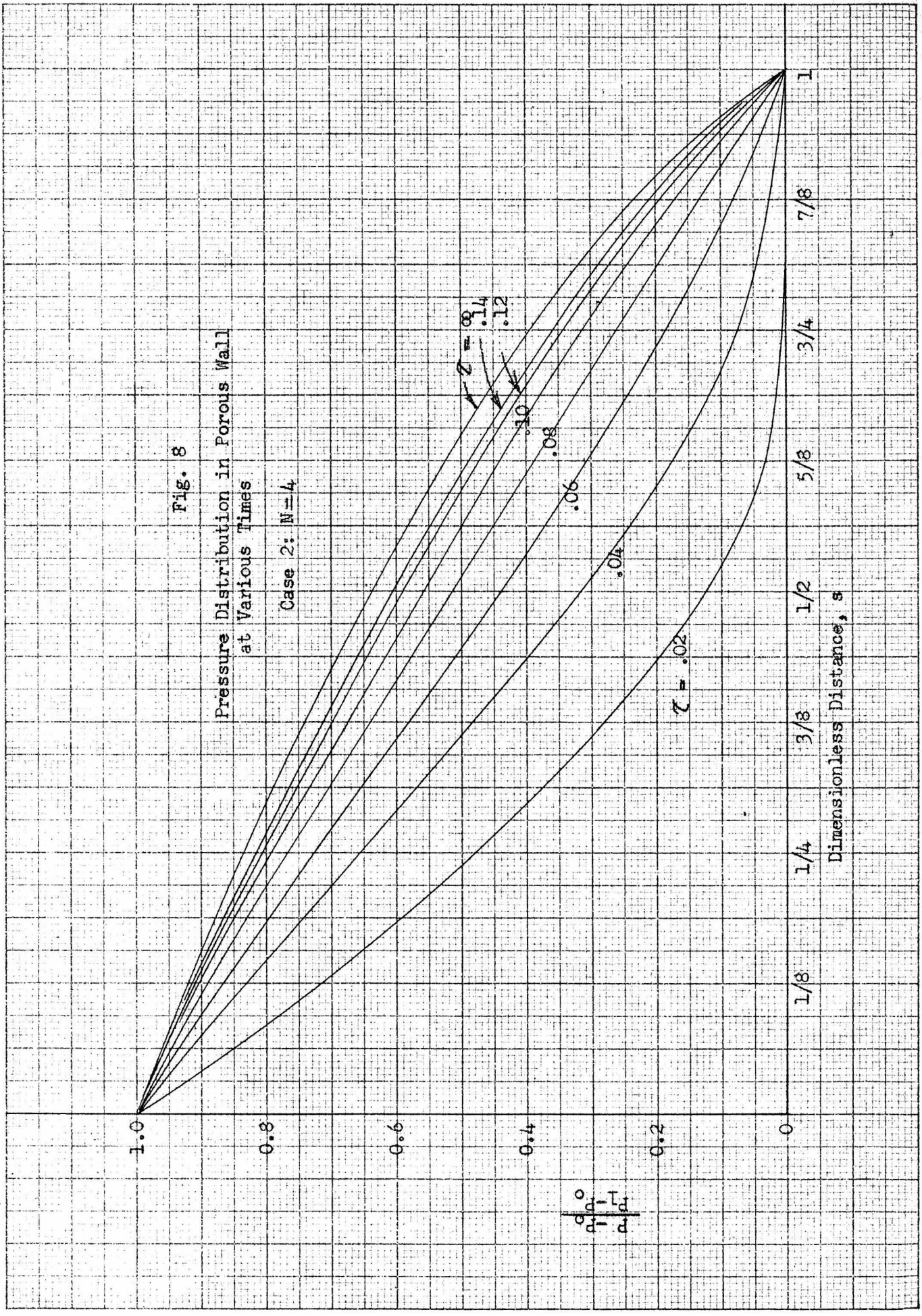
Fig. 8
Pressure Distribution in Porous Wall
at Various Times
Case 2: N=4
$\frac{p_0 - p}{p_0 - p_1}$
1.0
0.8
0.6
0.4
0.2
0
τ = .14
.12
.10
.08
.06
.04
τ = .02
1/8
1/4
3/8
1/2
5/8
3/4
7/8
1
Dimensionless Distance, s

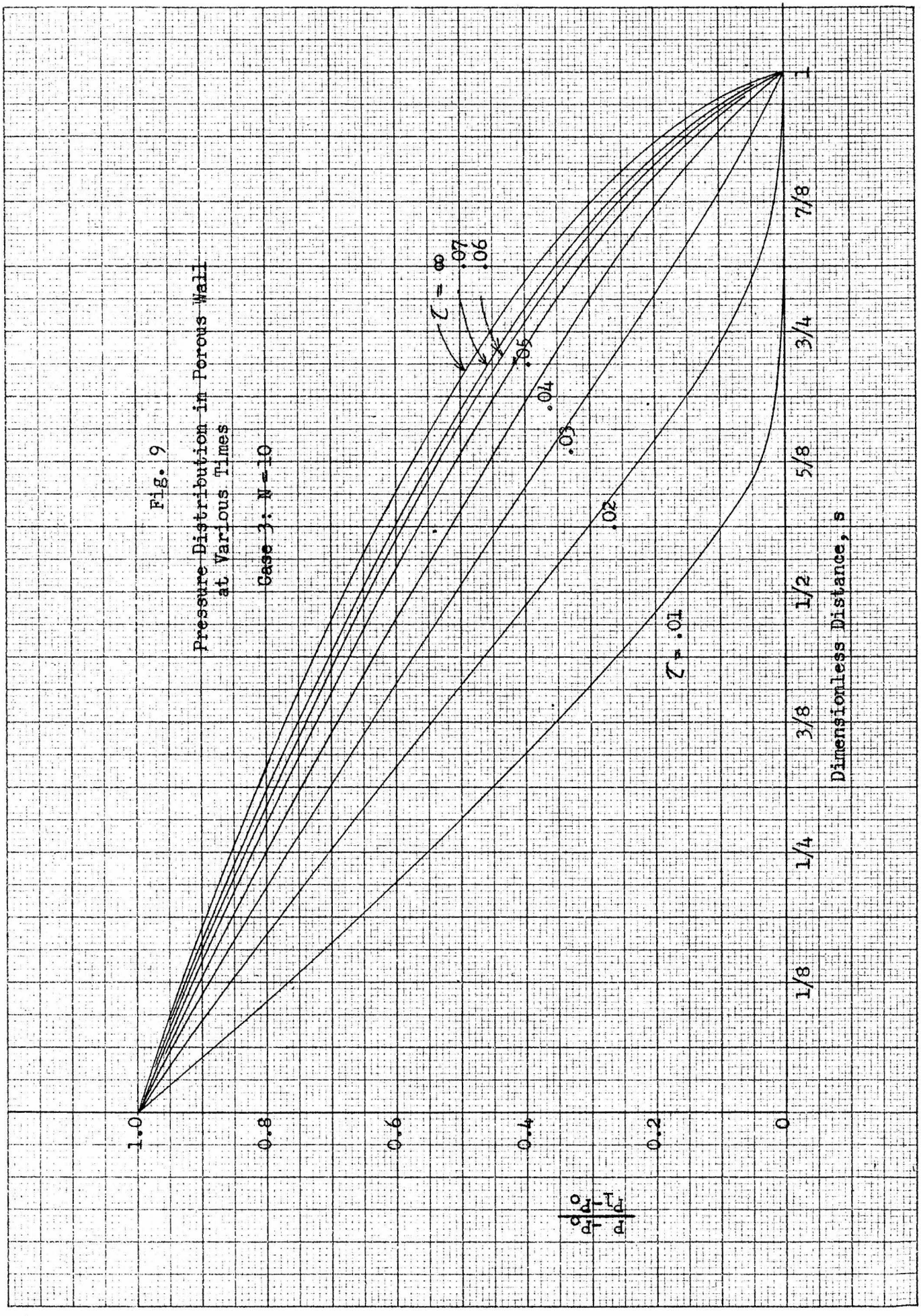
Fig. 9
Pressure Distribution in Porous Wall
at Various Times
Case 3: N=10
τ = ∞
.07
.06
.05
.04
.03
.02
τ = .01
1.0
0.8
0.6
0.4
0.2
0
1/8
1/4
3/8
1/2
5/8
3/4
7/8
1
Dimensionless Distance, s
$\frac{P_0 - P}{P_0 - P_1}$

Fig. 10

Dimensionless Pressure-Square Distribution in Porous Wall at Various Times

Case 1: N = 2

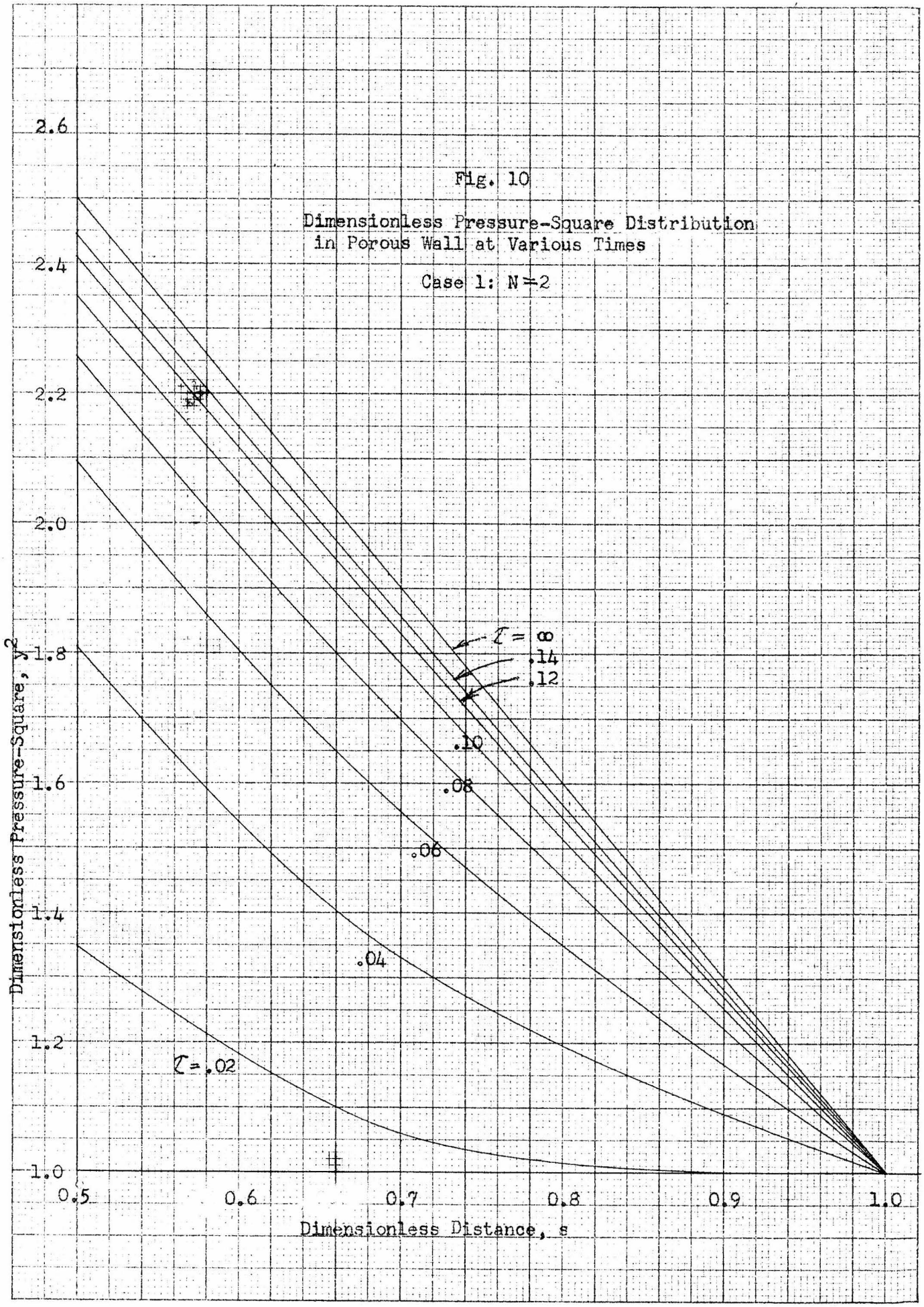

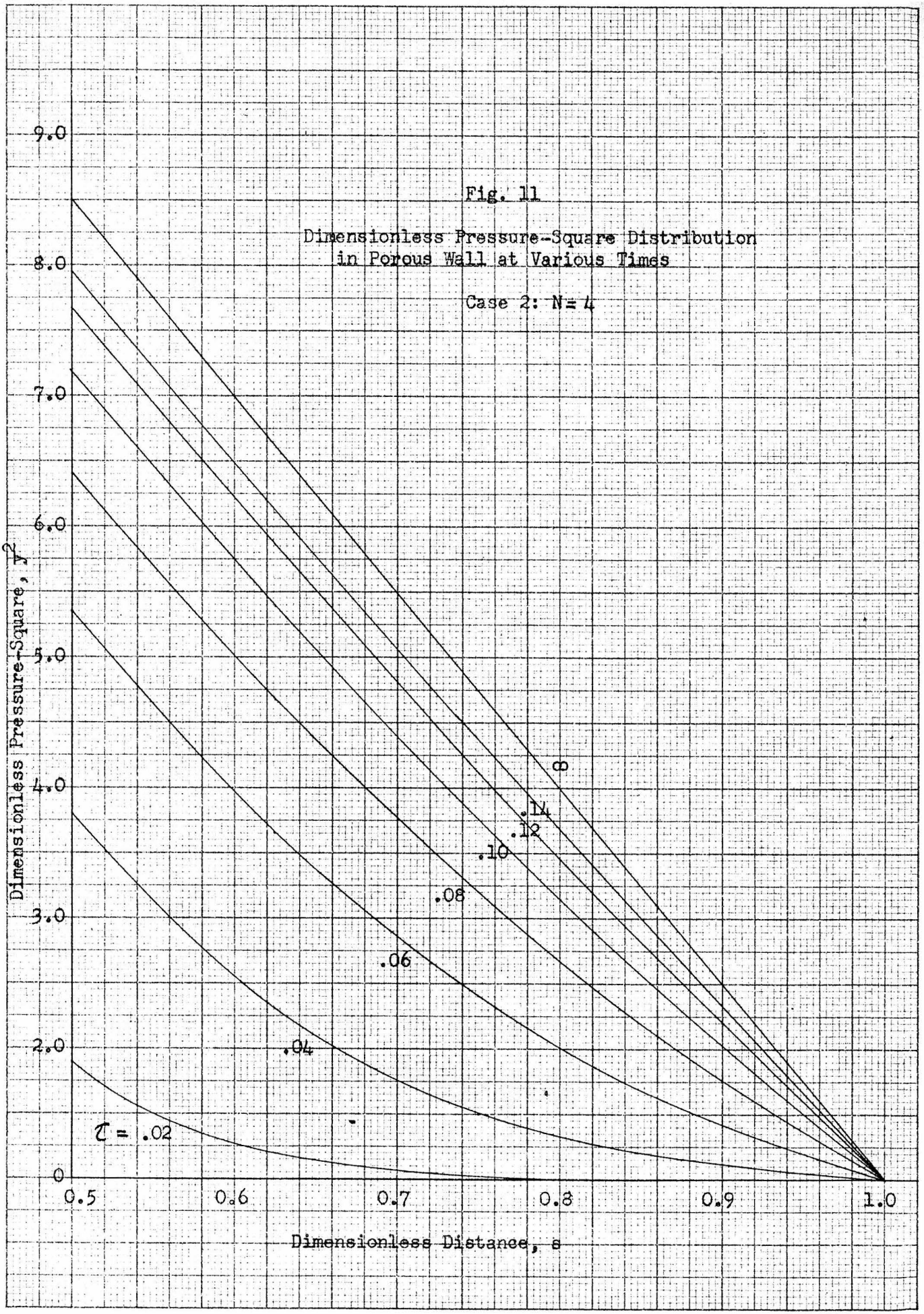

Fig. 11

Dimensionless Pressure-Square Distribution in Porous Wall at Various Times

Case 2: N = 4

Fig. 12

Dimensionless Pressure-Square Distribution
in Porous Wall at Various Times

Case 3: N=10

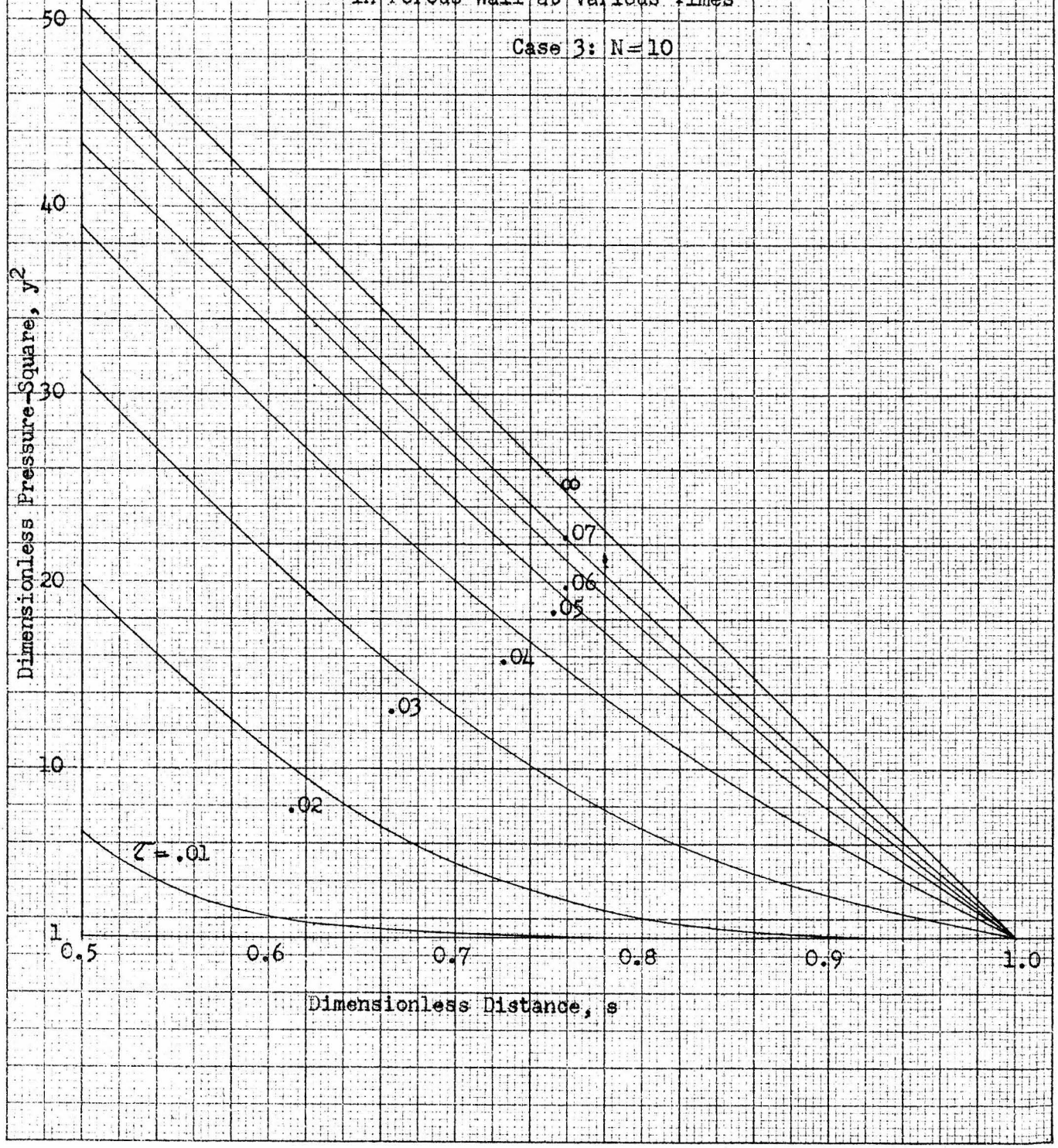

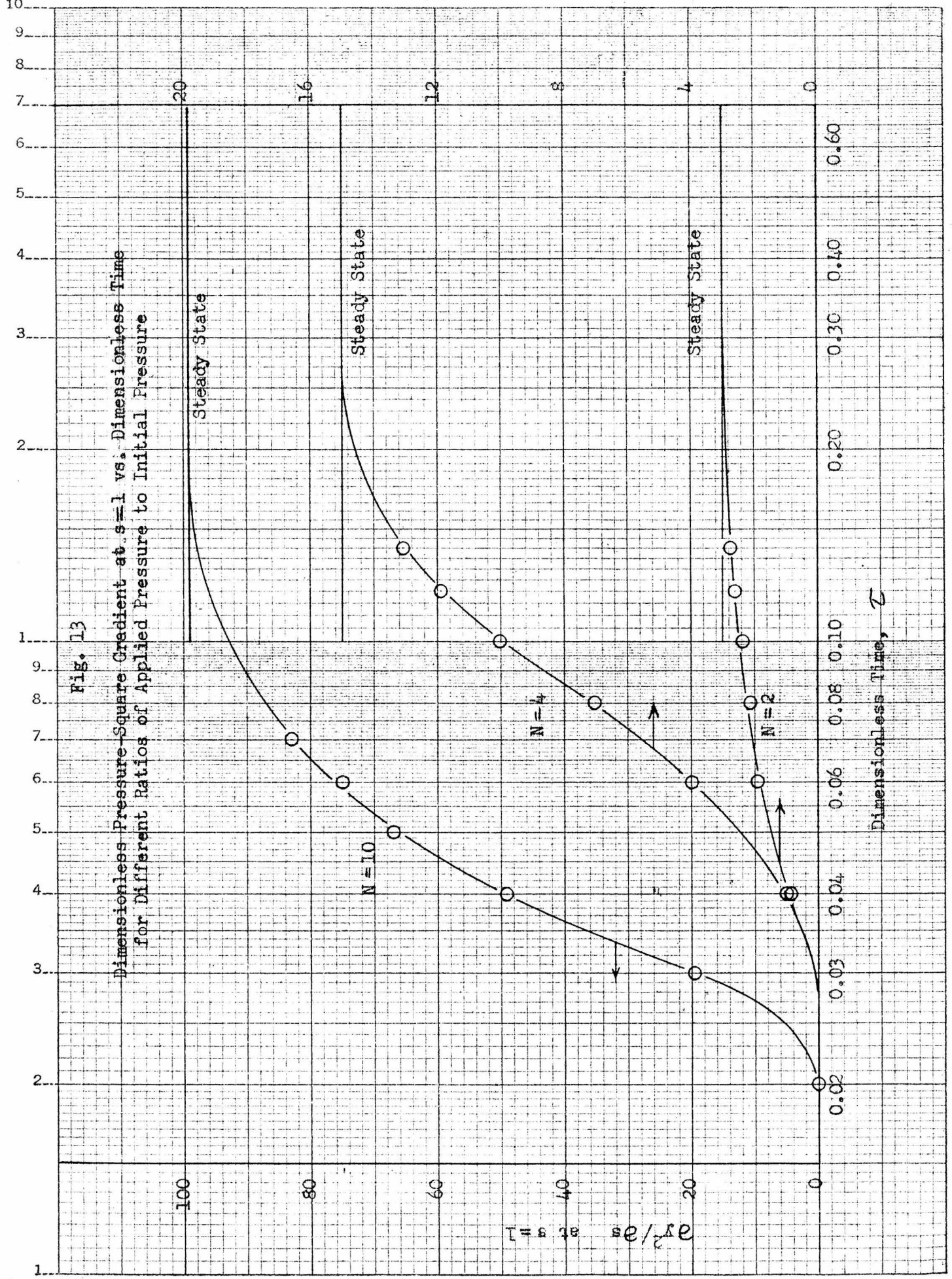

Fig. 13
Dimensionless Pressure-Square Gradient at $s=1$ vs. Dimensionless Time
for Different Ratios of Applied Pressure to Initial Pressure